NTNU – Trondheim
Norwegian University of
Science and Technology

Computer Controlled Dispersion Measurements and Investigation of New Optical Fibers

Alex Sembito

Condensed Matter Physics
Submission date: August 2014
Supervisor: Irina T Sorokina, IFY

Norwegian University of Science and Technology
Department of Physics

Abstract

A dispersion measurement setup for short length fibers based on Mach Zehnder interferometer was automatized and tested using standard telecommunication fiber. This setup is based on low coherence sources which enable interference to occur only in a narrow wavelength range. Dispersion in new optical fibers such as Ge-doped fiber and Yb:Tm doped fiber were measured over the wavelength range 1700nm-2400nm. Two broadband sources: - a superluminiscent Tm-doped fiber source (ASE source) and a modelocked Cr:ZnS oscillator were used for 1700nm-2000nm and 2150nm-2400nm wavelength ranges respectively. Manual measurements were first conducted before automation for comparison. During automation TRA25PPD stepper motor was used for position control and a CONEX IOD device was used to convert the analog signal from the oscilloscope into digital signal which was used to control the motor. A computer control program for the devices was written in the LabView environment. The setup is able to measure short length fibers of typically 40 cm - 250 cm. Different fiber lengths were tested to assess the measurement precision (70cm, 75cm and 207cm). The shorter the length, the less is the precision, although the results still remain in agreement with the results obtained using the long length fiber. The values of the measured second order dispersion coefficient were in agreement with the theoretically calculated values and provided a reasonable approximate of the dispersion in these fibers for areas of their applicability such as ultra-short pulsed lasers. The knowledge of second order dispersion in Germanate-doped fiber, Germanate-Tm and Yb:Tm doped fibers could further be used for development of novel ultra-short pulse fiber lasers operating in the 2µm spectral range.

Acknowledgement

Table of Contents

List of figures

ix

List of Tables

List of abbreviations

OF: Optical Fiber

ASE: Amplified Spontaneous Emission

CD: Chromatic Dispersion

PMD: Polarization Mode Dispersion

SMF: Single Mode Fiber

CSF: Conventional Single mode Fiber

NZ-DSF: NonZero-Dispersion Shifted Fiber

DGD: Differential Group Delay

TOF: Time Of Flight

MPS: Modulation Phase Shift

RF: Radio Frequency

OCT: Optical Coherence Tomography

DCF: Dispersion Compensating Fiber

DFF: Dispersion Flattened Fiber

MMF: Multi Mode Fiber

FWHM: Full Width at Half Maximum

LED: Light Emitting Diode

LCD: Liquid Crystal Display

QE: Quantum Efficiency

MP-NR: MultiPhonon-Non Radiative decay

MPR: Multi Phonon Relaxation

ADC: Analog to Digital Converter

CW: Continuous Wave

Chapter One: Introduction

1.0 Introduction

Optical fiber technology is one of the mostly developed techniques to transmit data with a very high bitrate. The technology uses the light source to encode the information signal and optical fiber as a signal transmission channel.

Information Signal becomes distorted due to attenuation and dispersion as it travels in an optical fiber. Group velocity dispersion (or simply 'dispersion') is the spreading of a signal pulse in the time domain as it travels through the fiber and attenuation is the loss of signal power due to absorption, scattering, and radiation. Due to dispersion, a pulse propagating down an optical fiber reaches their destination at slightly different times. This translates into a wider pulse at the receiving end of the fiber. Both attenuation and dispersion affect repeater spacing in a long distance fiber-optic communication system. Dispersion also affects the bandwidth of the system and maintaining low dispersion helps to ensure increased system information capacity, versatility and cost effectiveness.

1.1 Statement of the problem

Currently, there is a rapid development in the pulsed fiber laser systems and laser technology in the Mid-IR region. In order to develop ultra-short pulse laser systems in the mid IR, precise dispersion control is a necessity in order to achieve short and high quality pulses.

This research focuses on dispersion measurements in short length fibers using Mach Zhender interferometric technique. Because usually for investigation and study purposes, long length optical fibers are not available, thus a fast and reliable dispersion measurement setup suitable for the short length fibers is required. Due to inconsistency, time consumption and unreliability of the manual setup results, automation of the setup is required. As such, the main goal of the present work is automation of the dispersion measurement setup for measurement of the short pieces of fibers and bulk solid-state materials. Another goal of the work is making the setup compact and reliable.

Efficient light sources for pumping the experiment in the wavelength region of interest are not available on market, hence a need to make such a laser source. The light sources available on market such as the LEDs and semiconductors have high coupling losses into the fiber and are

temperature dependent.

The setup implements two broadband light sources in the mid infrared region:- ASE source based on Tm doped fiber and femtosecond Cr:ZnS laser which differentiates the setup from the other existing dispersion measuring setups.

As a result of the project, we shall have a reliable dispersion setup that can be put in a compact box and could be used for short length dispersion measurement.

1.2 Specific objectives

In order to achieve the main goals in the statement of the problem above, the following objectives are accomplished.

(i) Making an ASE source based on Tm-doped fiber.

(ii) Measurement of dispersion in several specialty fibers using the existing novel manual setup based on Mach Zehnder Interferometer using superluminescent Tm-doped fiber based source(ASE) and a mode-locked femtosecond Cr:ZnS oscillator laser for 1.7 to 2.0 and 2.3 to 2.45 microns respectively

(iii) Computerization of the setup using position controllers such as stepper motors and digital signal converters.

(iv) Measurement of dispersion in optical fibers using the automated setup

(v) Comparison of the results from the manual and automated setup

(vi) Determine the Shortest fiber lengths that can be measured by the setup

These objectives will not only lead to the fully computer controlled dispersion setup but also will explore the limits of increasing the compactness of the setup since reducing the fiber lengths will reduce the air paths length. Also shorter fibers reduce costs especially for very expensive optical fibers.

1.3 Scope of the study

This research focuses on dispersion measurement on short length optical fibers based on a Mach Zhender interferometer setup in the near and mid infrared region with computerization as the major emphasis. Dispersion measurement in specialty fibers is very critical in the 1.7-2.5

microns especially for fibers used to make ultra-short fiber lasers in this wavelength range
Precise dispersion control is absolutely necessary in order to achieve sub-picosecond laser pulses.

Also the focus is in infrared because of the wide range of applications in this wavelength region. This includes medical applications and industrial applications. Increasing the bitrate of the telecommunication systems will result in the thorough research on transmission systems within this wavelength range. The emission sources used in the project are new broadband light sources; - superluminescent Tm-doped fiber based source (ASE) and a mode-locked femtosecond Cr:ZnS oscillator. These broadband sources emit in the wavelength ranges 1.7 to 2.0 and 2.3 to 2.45 microns respectively.

Chapter Two: Literature Review

2.0 Introduction

Optical fiber investigation has been one of the important research areas in fiber optics. New fiber optic materials with low transmission losses and ultra-short pulsed laser sources have been among the major areas research. This chapter focuses on dispersion in optical fibers in the near and mid-infrared region and laser sources emitting in such wavelength region.

2.1 Dispersion in optical fibers.

Dispersion is the tendency of the pulse to broaden in an optical fiber during transmission. It limits the quality of the signals transmitted over an optical communication network. Dispersion affects the quality of ultra-short pulsed laser systems. It is a result of the physical properties of the transmission medium. Single mode fibers normally used for high speed signal transmission are typically subject to Chromatic Dispersion (CD) and Polarization Mode dispersion (PMD). Chromatic dispersion causes broadening of the pulse depending on wavelength while Polarization Mode Dispersion causes pulse broadening depending on polarization. The broadening of the pulses during transmission can cause encoded bits of data to overlap with each other which lead to an increase in the bit error rate. Thus there is always a need to control dispersion in order to operate in the regime where dispersion is minimal (close to zero). Figure 1 below shows how the encoded signal at the output of a transmission channel gets affected by dispersion and attenuation.
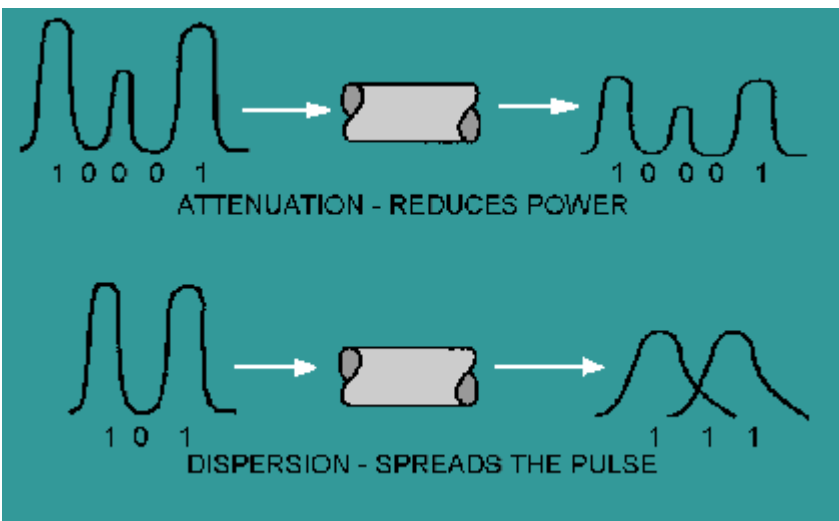
Figure 1: Concept of dispersion and attenuation [1]

2.1.1 Dispersion in Single-Mode Fibers

Single mode fibers are fibers that are designed to transmit only one mode. Dispersion in single-mode fibers is due to intramodal dispersion (also known as chromatic dispersion where different wavelengths travel at different speeds arriving at different times as shown in Figure 2) and polarisation mode dispersion. Chromatic dispersion is due to two dispersion mechanisms; -material dispersion and waveguide dispersion.
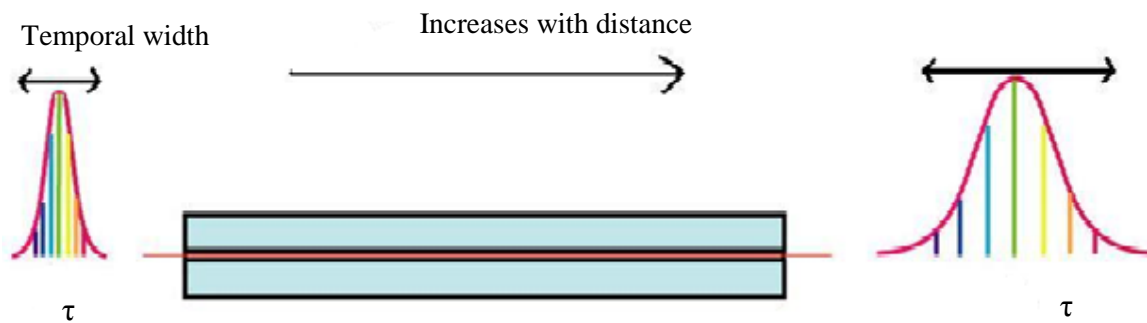
Figure 2: Chromatic dispersion in single-mode fiber (different wavelength travel at different speeds in the optical fiber) [2]

Chromatic dispersion is expressed in units of ps/nm*km which shows the pulse spreading in time (in ps) for a pulse with spectral width of 1nm travelling over 1km distance inside the fiber. Chromatic dispersion depends on the fiber type and it is the most dominant dispersive mechanism in single mode fibers. The chromatic dispersion mechanisms and other mechanisms are described below.

Material Dispersion

Material dispersion is caused by variations of refractive index of the fiber material with respect to wavelength. Since the group velocity is a function of the refractive index, the spectral components of any given signal will travel at different speeds causing deformation of the pulse. Variations of refractive index with respect to wavelength are described by the Sellmeier equation which is

expressed as [3]

$$n(\lambda) = [1 + \sum_{i=1}^{3} [\frac{A_i \lambda^2}{(\lambda^2 - \lambda_i^2)}]^{\frac{1}{2}}] \qquad (1)$$

Where λ is the wavelength of light, and A_i and λ_i are the Sellmeier coefficients, and are tabulated in [3] and [4] for a number of silica-based glass materials commonly used in fabrication of optical fibers.

Material dispersion coefficient

In order to derive the material dispersion coefficient, let us for simplicity consider,

$$v_g = \frac{c}{n_g} \qquad (2)$$

Where v_g is the group velocity, n_g the group refractive index of the material, c is the speed of light in the vacuum.

The group refractive index of the material is given by:-

$$n_g = n(\lambda_o) - \lambda_o \frac{dn}{d\lambda_o} \qquad (3)$$

$n(\lambda_o)$ is refractive index which depends on wavelength

It is clear that for each λ_o, v_g changes. Thus such dispersion that arises from material properties of the fiber is called material dispersion

If we assume an optical pulse to be a Gaussian beam of spectral width σ_λ after travelling a distance L in a dispersive material, its temporal duration is given by:-

$$\sigma_\tau = \left| \left(\frac{d}{d\lambda_o} \right) \left(\frac{L}{v_g} \right) \right| \sigma_\lambda \qquad (4)$$

Putting equation (2) in (4), we obtain:-

$$\sigma_\tau = \left| \left(\frac{d}{d\lambda_o} \right) \left(\frac{Ln_g}{c} \right) \right| \sigma_\lambda \qquad (5)$$

Putting equation (3) in (5)

$$\sigma_\tau = \left| -\frac{\lambda_o}{c} \frac{d^2 n}{d\lambda_o^2} \right| L\sigma_\lambda \qquad (6)$$

We can thus write the pulse duration as:-

$$\sigma_\tau = |D_m| L\sigma_\lambda \qquad (7)$$

Where

$$D_m = -\frac{\lambda_o}{c}\frac{d^2n}{d\lambda_o^2} \hspace{6cm} (8)$$

D_m is called the material dispersion coefficient

The table 1 below shows typical material dispersion coefficients for pure silica.

λ_0 (μm)	n (λ_0)	$\frac{dn}{d\lambda_0}\mu m^{-1}$	n_g (λ_0)	$\frac{d^2n}{d\lambda_0{}^2}\mu m^{-2}$	D_m (ps/nm·km)
0.70	1.45561	−0.02276	1.47154	0.0741	−172.9
0.75	1.45456	−0.01958	1.46924	0.0541	−135.3
0.80	1.45364	−0.01725159	1.46744	0.0400	−106.6
0.85	1.45282	−0.01552236	1.46601	0.0297	−84.2
0.90	1.45208	−0.01423535	1.46489	0.0221	−66.4
0.95	1.45139	−0.01327862	1.46401	0.0164	−51.9
1.00	1.45075	−0.01257282	1.46332	0.0120	−40.1
1.05	1.45013	−0.01206070	1.46279	0.0086	−30.1
1.10	1.44954	−0.01170022	1.46241	0.0059	−21.7
1.15	1.44896	−0.01146001	1.46214	0.0037	−14.5
1.20	1.44839	−0.01131637	1.46197	0.0020	−8.14
1.25	1.44783	−0.01125123	1.46189	0.00062	−2.58
1.30	1.44726	−0.01125037	1.46189	−0.00055	2.39
1.35	1.44670	−0.01130300	1.46196	−0.00153	6.87
1.40	1.44613	−0.01140040	1.46209	−0.00235	10.95
1.45	1.44556	−0.01153568	1.46229	−0.00305	14.72
1.50	1.44498	−0.01170333	1.46253	−0.00365	18.23
1.55	1.44439	−0.01189888	1.46283	−0.00416	21.52
1.60	1.44379	−0.01211873	1.46318	−0.00462	24.64

Table 1: Variation of refractive index with wavelength for pure silica [5]

It is thus clear from equation (8) and table 1 that material dispersion is dependent on refractive index of medium and the wavelength. This coefficient generally increases with wavelengths for typical silica fiber and it can be negative (normal dispersion where the longer wavelengths travel faster than the shorter ones) or positive (anomalous dispersion where the short wavelengths travel faster than the long ones), as shown in Figure 3 below.
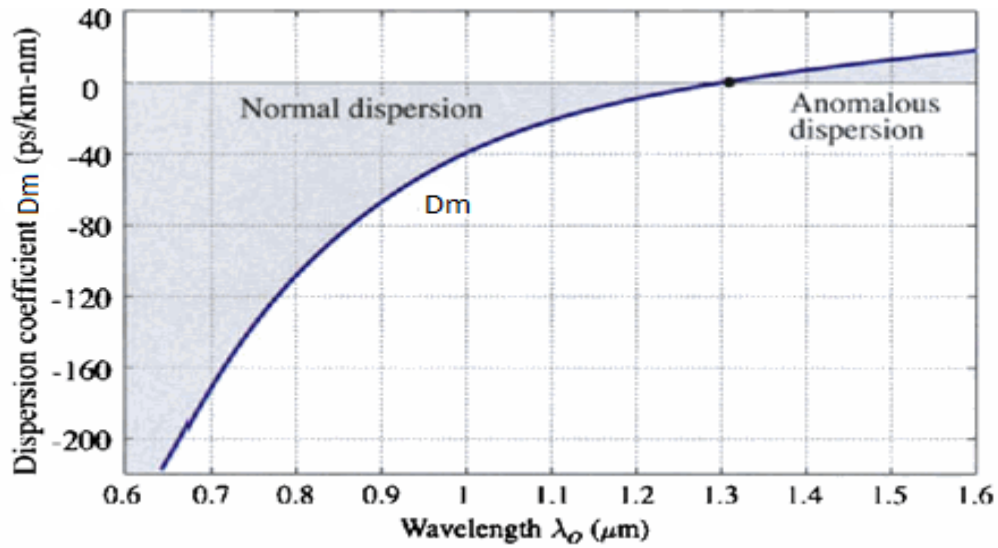
Figure 3: Material dispersion coefficient as a function of wavelength for silica fiber [6]
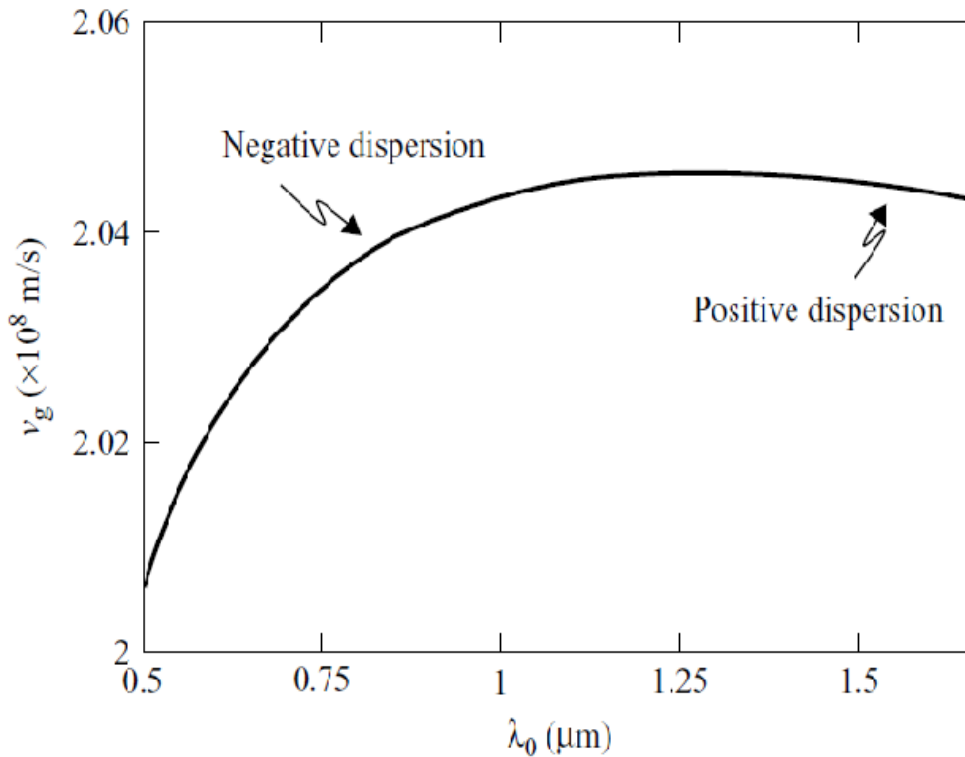
Figure 4: Wavelength dependence of group velocity for pure silica fiber [5].

The group velocity of the silica fiber is dependent on the wavelength as shown in Figure 4 above. It attains its maximum at around 1.27µm (Figure 5). At this point dispersion coefficient

is equal to zero, therefore this is called zero dispersion wavelength, particularly important in optical communications. Fibers with zero total dispersion at about 1270 nm are known as conventional single-mode fibers (CSF) or according to telecommunication standards as G.652 fibers. For some fibers, the zero wavelengths has been shifted to about 1500nm, where the loss is lowest. Such fibers are known as dispersion-shifted fibers (DSFs) or G.653 fibers according to the telecommunication standards. There are other fibers that are designed so that they have a non-zero finite dispersion at around 1550nm, and they are referred to as the nonzero-dispersion-shifted fiber (NZ-DSF). This is to ensure that there is no nonlinear mixing (also referred to as four-wave mixing between various wavelength channels. Such fibers are referred to as G.655 fibers [5]. These telecom fibers have different chromatic dispersion. Typical examples are shown in Figures 5-8, where D_m is the material dispersion coefficient, D_w is the waveguide dispersion coefficient and D_t is the total dispersion coefficient [6]. The zero dispersion wavelength changes depending on the fiber parameters.
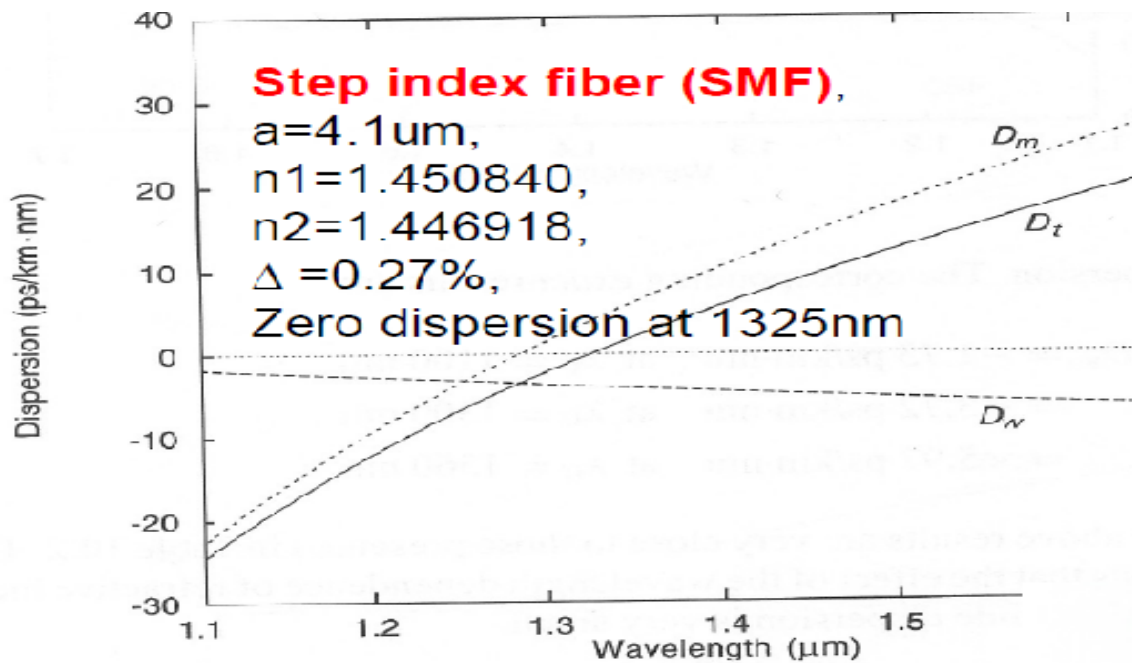
Figure 5: Chromatic dispersion in a conventional single mode fiber [6]
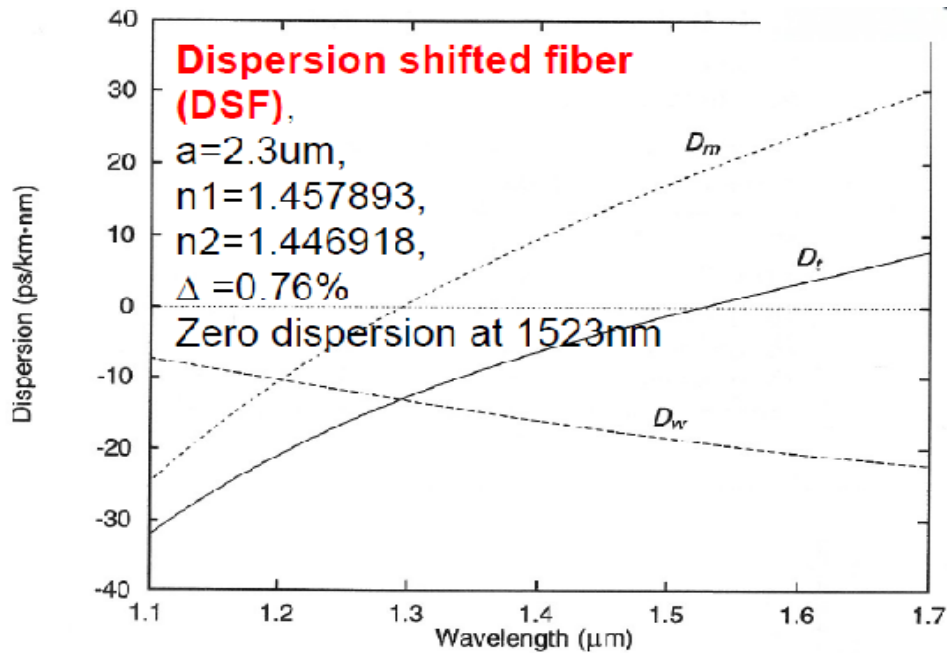
Figure 6: Chromatic dispersion in dispersion shifted fiber [6]
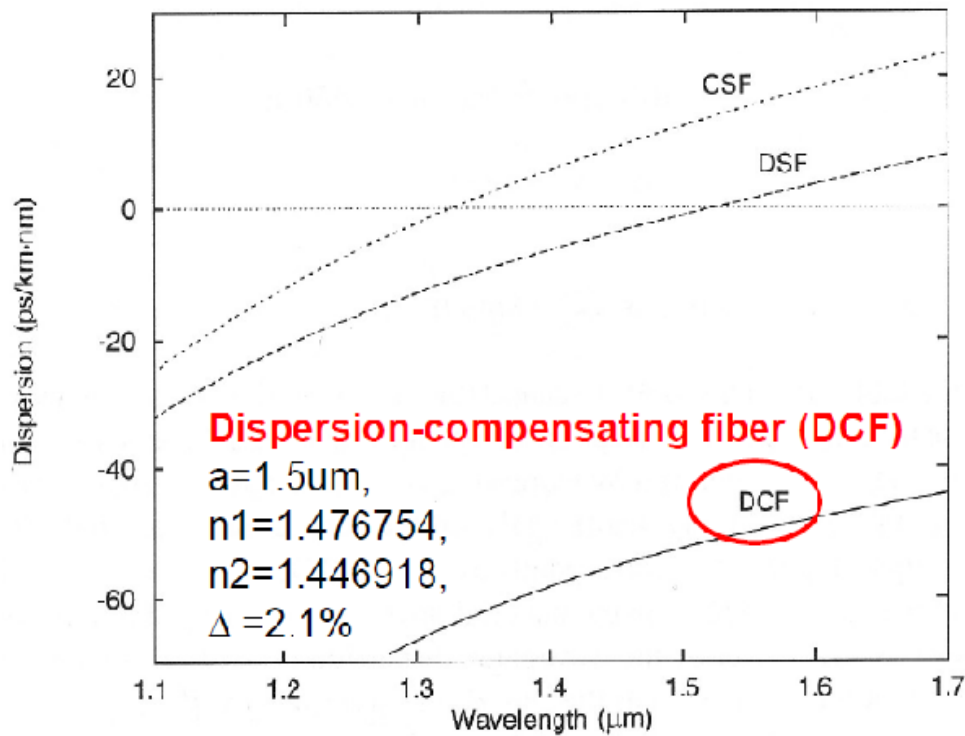
Figure 7: Chromatic dispersion in dispersion compensating fiber [6]
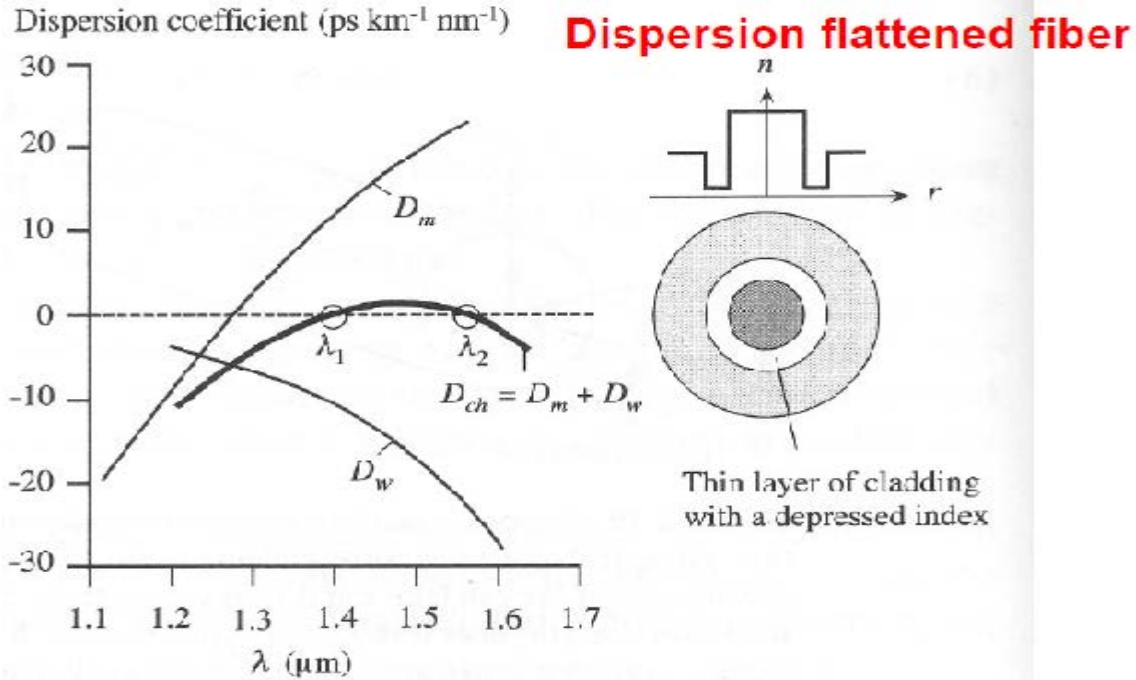
Figure 8: Chromatic dispersion in dispersion flattened fiber [6]

The wavelength dependence of dispersion of a single-mode fiber in the wavelength range 1200-1625nm can be estimated using the following relation [5];-

$$D(\lambda) = \frac{S_o}{4}\left(\lambda - \frac{\lambda_o^4}{\lambda^3}\right) \qquad (9)$$

Where S_o is the slope from the dispersion curve, λ_o is the zero dispersion wavelength of the fiber and λ is the wavelength of interest. Table 2 contains the dispersion coefficients and their slopes for some standard fibers at 1500nm

Fiber Type	D (ps/km·nm)	S (ps/km·nm^2)
Standard SMF (G.652)	17	0.058
LEAF (Corning)	4.2	0.085
Truewave-reduced slope (OFS)	4.5	0.045
TeraLight (Alcatel)	8.0	0.057

Table 2: Values of dispersion and dispersion slopes for some standard silica fibers at 1550nm [5]

Waveguide Dispersion

Waveguide dispersion occurs due to different spectral components of a pulse travelling with different velocities within the fiber. It is a result of axial propagation constant β being a function of wavelength due to the existence of one or more boundaries in the structure of the fiber. Thus eliminating such boundaries, the fiber reduces to a homogeneous medium, the fundamental mode becomes a uniform plane-wave, and the waveguide dispersion effect is eliminated.

Waveguide dispersion coefficient

As seen before, the temporal duration or pulse broadening of a Gaussian beam can be written as:

$$\sigma_\tau = \left| \left(\frac{d}{d\lambda_o} \right) \left(\frac{L}{V_g} \right) \right| \sigma_\lambda \tag{10}$$

But $\dfrac{1}{v_g} = \dfrac{d\beta}{d\omega} = \dfrac{d\beta}{dV} \dfrac{dV}{d\omega} = \dfrac{a.NA}{c_o} \dfrac{d\beta}{dV}$, $\tag{11}$

Where

$$V = 2\pi \left(\frac{a}{\lambda_o} \right) NA = \frac{a.NA}{c_o} \omega \tag{12}$$

We can thus write,

$$\sigma_\tau = |D_w| L \sigma_\lambda \tag{13}$$

Where the waveguide dispersion coefficient is given by

$$D_w = \frac{d}{d\lambda_o} \left(\frac{1}{v_g} \right) = -\frac{\omega}{\lambda_o} \frac{d}{d\omega} \left(\frac{1}{v_g} \right) \tag{14}$$

Putting (11) in (14) we obtain

$$D_w = -\left(\frac{1}{2\pi c_o} \right) V^2 \frac{d^2\beta}{d^2V} \tag{15}$$

Since V-number is a function of wavelength, λ_o, and radius of the core, a, the waveguide dispersion coefficient D_w is thus also a function of λ_o, *and a*. This means that the waveguide dispersion can be controlled by altering the radius of the core for a step index fiber and for the graded index fibers, by altering the index grading profile [6]

The waveguide dispersion D_w in a step-index single-mode fiber can be approximated by the expression [7]

$$D_w = -\frac{n_2\Delta}{3\lambda_o} \times 10^7 [0.080 + 0.549(2.834 - V)] \text{ ps/km.nm} \tag{16}$$

Where V is the V-number, n_2 is the refractive index of the cladding and λ_o is measured in nm

The negative sign indicates that longer wavelengths travel faster than shorter wavelengths.

The total chromatic dispersion in singe mode fibers is given by the sum of material and waveguide dispersions (Figure 9).

$$D_{tot} = D_m + D_w \qquad\qquad (17)$$

Dispersion ps/km/nm as a function of Wavelength
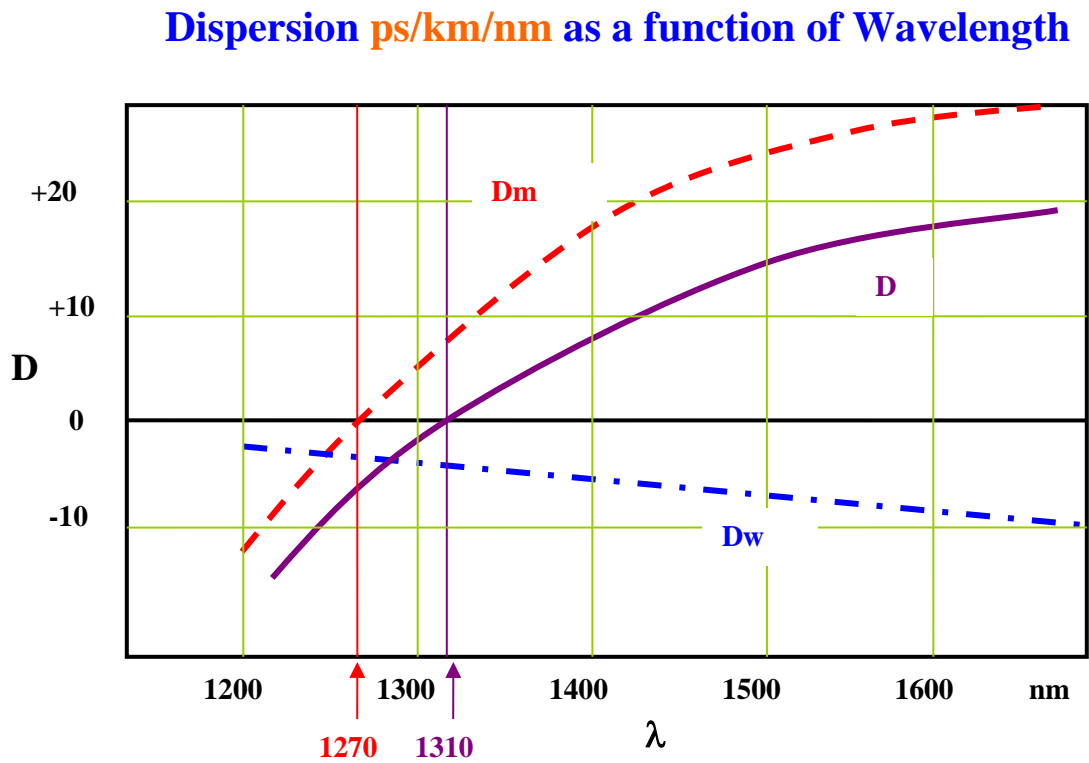
Figure 9: Variation of material, waveguide and total dispersion for a standard single mode silica fiber [8]

The material dispersion is zero at 1270nm for standard silica single mode fiber. But due to the fact that chromatic dispersion is a result of material and wave guide dispersion, the total dispersion is zero at 1310nm as shown in Figure 6.

Polarization-Mode Dispersion

Polarization-mode dispersion is a result of the time difference in the group delays between the two orthogonal polarized modes which leads to pulse broadening.

Single-mode fibers, in reality, support two orthogonally-polarized fundamental modes. In perfectly circular fibers, these two modes have identical propagation constants (i.e. propagate at the same velocity) and pulse spreading due to polarization-mode dispersion does not exist. In practice however, perfect circular fibers do not exist, thus there is a small difference between the propagation constants of these two modes due to the non-circular behavior of the core. Thus single-mode fibers actually support two modes and thus are not truly single-mode. These two fundamental modes contribute to pulse broadening. The amount of pulse spreading caused by the difference in speeds of the principal modes is called differential group delay (DGD) and it's measured in picoseconds (Figure 10) [9].

Polarization Mode Dispersion
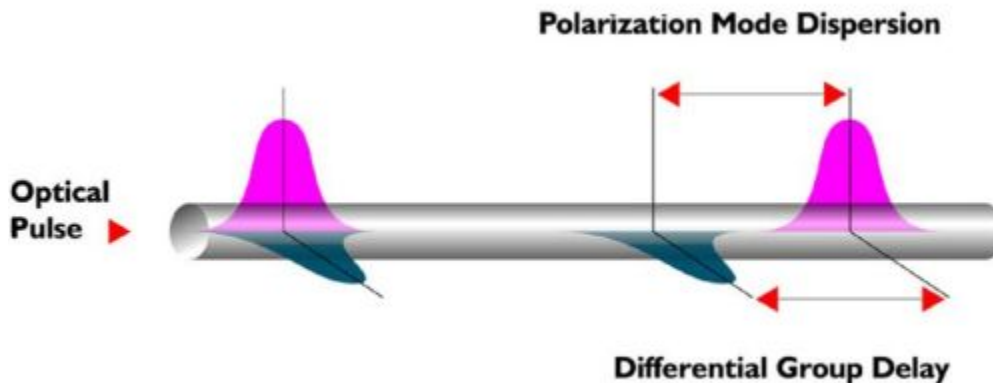
Figure 10: Polarization mode dispersion in single mode optical fibers [9]

In addition to fiber geometry, PMD is also created by external forces such as bends, twists, and stress.

2.1.2 Dispersion in Multimode Fibers

Multimode fibers are fibers that are designed to transmit more than one mode. In applications where two or more modes travel simultaneously through the fiber, both intermodal (modal) and intramodal dispersions exist.

Intermodal (or modal) dispersion

Intermodal dispersion is significant effect in multimode fibers. It occurs as a result of different modes having different group velocities at the same frequency. The intermodal effect has significantly been reduced by using graded index fibers with almost parabolic index profile. The bound rays that deviate from the axis travel a bit longer distance but instead at higher velocities thus arriving at the receiving end of the fiber nearly at the same time with all the other rays, hence reducing the spreading of the rays (Figures 11, 12).
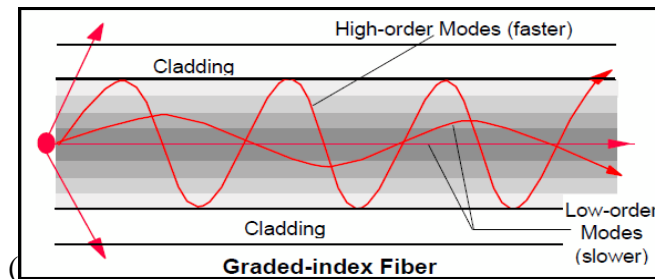
Figure 11: Mode propagation in a graded index fiber [5].
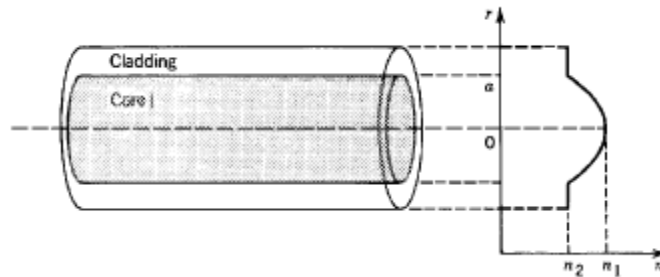
Figure 12: Refractive index profile of graded index fiber [5]

Consider a single pulse entering an N- mode fiber, which spreads into N pulses whose differential delay increases as a function of fiber length L (Figure 13). The time delays for the different velocities are obtained from $\tau_m = \frac{L}{v_m}$, m=1, 2.............N, where v_m is the group velocity of the mth mode. Thus, if τ_{min} corresponding to v_{max} and τ_{min} corresponding to v_{min} are the minimum and the maximum time delays, where v_{min} and v_{max} are the smallest and the largest group velocities respectively, the received pulse will spread over a time interval $\tau_{max} - \tau_{min}$.

15

Thus the overall pulse duration assuming a triangular envelop and using Full Width at Half Maximum (FWHM) definition can be estimated as [6]:

$$\sigma_\tau = \frac{1}{2}\left(\frac{L}{V_{min}} - \frac{L}{V_{max}}\right) = \frac{1}{2}(\tau_{max} - \tau_{min}) \tag{18}$$

σ_τ represents the modal dispersion response time of the fiber
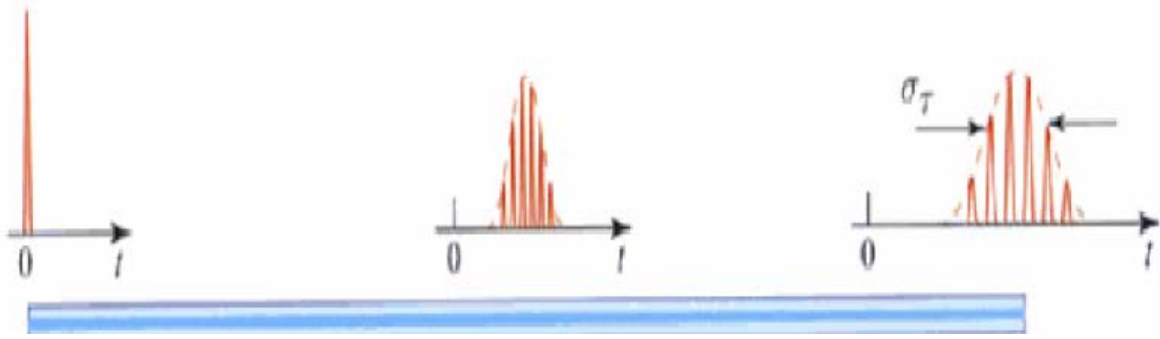
Figure 13: Pulse spreading caused by modal dispersion [6]

Typically for a step index fiber with a large number of modes, $v_{min} \approx c_1(1 - \Delta)$ and $v_{max} \approx c_1$. The response time is thus:

$$\sigma_\tau \approx \frac{L}{c_1} \cdot \frac{\Delta}{2} \tag{19}$$

Thus the response time is a fraction $\frac{\Delta}{2}$ of the delay time $\frac{L}{c_1}$

Comparing the modal dispersion for the step index optical fiber and that of the graded index fibers, it turns out that it is a smaller effect in graded index fiber than the step index fiber. This is because the group velocities are equalized and the differences between the delay times of the modes are reduced. For a graded index fiber with a large number of modes, $v_{min} \approx c_1\left(1 - \frac{\Delta^2}{2}\right)$ and $v_{max} \approx c_1$ and this results into a response time with a factor $\frac{\Delta}{2}$ smaller than that in a step index optical fiber.

$$\sigma_\tau \approx \frac{L}{c_1} \cdot \frac{\Delta^2}{4} \tag{20}$$

16

From the response time equations for both the step index and graded index fiber, it can be seen that the response time is proportional to length L. But typically we have coupling between the modes, thus such dependence of response time with length L, is valid for fibers not longer than the critical length. When the critical length is exceeded, the response time σ_τ will be proportional to $\sqrt{L}$ thus reducing the pulse broadening.

Coupling of the modes is a result of the imperfections of the fiber or the inhomogeneities in the refractive index which facilitate the coupling of the modes that have nearly the same propagation constant allowing exchange of the optical power between the modes.

Material dispersion is the only significant intramodal effect for fibers with standard geometry, so waveguide dispersion can be neglected for such fibers. Thus, pulse spreading in multimode fibers is largely due to material dispersion and intermodal delay distortion. Polarization-mode dispersion is a much weaker effect than material dispersion and intermodal delay, and is often neglected in the analysis and design of fiber optic links [10].
.

2.2 Dispersion measurement techniques

There are several techniques used to measure dispersion. The choice depends on several factors like precision, the length of the fiber to be measured, the type of pumping source for the experiment.These measurement techniques include:

- Time-Of-Flight technique
- Modulation Phase-Shift
- Interferometric techniques
- Degenerate-Four-Wave-Mixing-based techniques.

Detailed discription of the methods is given below.

2.2.1 Interferometric techniques

These techniques can be divided into Fourier transform methods (Temporal interferometry) and non-Fourier transform methods (spectral interferometry).

The Non-Fourier transform methods can be employed by using direct techniques (turning point

analysis) or indirect techniques (shift of center wavelength when optical path length changes or center wavelength against air paths length) while the Fourier- transform methods are employed by Fourier-transforming the interferogram [11, 12].

Non Fourier-transform methods involve the use of a tunable laser source since the output intensity of the interferometer is measured at several wavelengths at a constant distance between the air paths length and arm with the fiber under test or at variable distance between the air paths length and arm with the fiber under test. On the other hand, Fourier transform method requires a broad band laser source and does not involve varying wavelengths when varying the differences between the air arm and that of fiber under test.

The dispersion parameter and the slope of the fiber under test can be obtained by using the fiber parameters and from the relations [11, 13]

$$D(\lambda) = \frac{dn_g(\lambda)}{Cd\lambda} = -\frac{\lambda d^2 n(\lambda)}{Cd\lambda^2} \tag{21}$$

$$S(\lambda) = \frac{dD(\lambda)}{d\lambda} = -\frac{\lambda d^3 n(\lambda)}{Cd\lambda^3} + \frac{1}{\lambda}D(\lambda) \tag{22}$$

Dispersion measurement using Non-Fourier -transform methods

These methods are divided into direct and indirect techniques.

Typical example of Non Fourier- transform method is a Mach Zhender based interferometric setup (Figure 14). In a Mach Zhender interferometer, a beam of light from a laser source is split into two by abeam splitter. One beam goes into the air arm and the second beam into the fiber arm. The two beams propagate differently due to the difference in the propagation properties of media (the air and the fiber) which results into interference fringe patterns. The two beams then recombine using a beam combiner and then directed to the detector. The signal at the detector changes as the wavelength changes the fiber optical path length is wavelength dependent. Thus for a particular wavelength, the variable arm can be adjusted to equalize the two beams for maximum interference to occur (indirect technique).
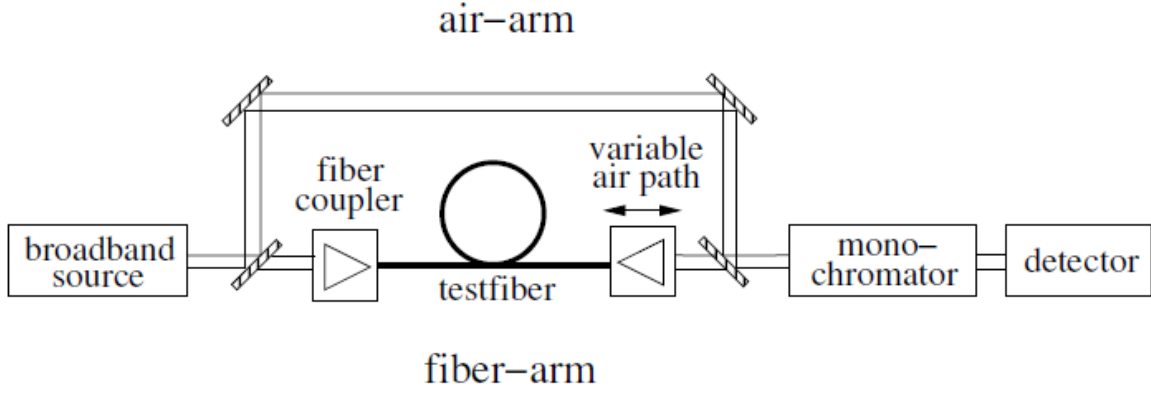
Figure 14: Simple Mach Zehnder Interferometric setup [11]

Let us consider a test fiber of length, L_{fiber} in a Mach Zehnder Interferometer where the air arm is $L_{air-arm}$. Due to the fact that there exists air-paths in the fiber arm $L_{air,fiber-arm}$, this has to be subtracted from the length of the air arm to get the path length. Thus,

$$L_{air} = L_{air-arm} - L_{air,fiber-arm} \tag{23}$$

The resulting optical path difference (OPD) between the air arm and the fiber arm is then given by:-

$$OPD = L_{air} - n(\lambda)L_{fiber} \tag{24}$$

Signal analysis at the detector

The intensity of the two beams after recombining can be expressed as a superposition of the intensity of the fiber arm and air path arm

$$I_{out}(\lambda) = I_{air}(\lambda) + I_{fiber}(\lambda) - 2\sqrt{(I_{air}(\lambda)I_{fiber}(\lambda)}\cos[\frac{2\pi}{\lambda}(L_{air} - n(\lambda)L_{fiber})]) \tag{25}$$

On the other hand, expanding the refractive index about the center wavelength λ', we obtain

$$n(\lambda) = n' + (\lambda - \lambda')\frac{dn}{d\lambda} + \frac{(\lambda-\lambda')^2}{2!}\frac{d^2n}{d\lambda^2} + \frac{(\lambda-\lambda')^3}{3!}\frac{d^3n}{d\lambda^3} + \cdots \tag{26}$$

19

Substituting equation (26) in (25), we obtain

$$I_{out}(\lambda) = I_{air}(\lambda) + I_{fiber}(\lambda) - 2\sqrt{(I_{air}(\lambda)I_{fiber}(\lambda)} \cos\left[\frac{2\pi}{\lambda}\left(L_{air} - L_{fiber}\left(n' - \lambda'\frac{dn}{d\lambda}\right)\right) - \right.$$

$$\left. 2\pi I_{fiber}\left(\frac{dn}{d\lambda} + \frac{(\lambda-\lambda')^2}{2!\lambda}\frac{d^2n}{d\lambda^2} + \frac{(\lambda-\lambda')^3}{3!\lambda}\frac{d^3n}{d\lambda^3} + \cdots\right)\right] \tag{27}$$

But at the center wavelength, the group propagation time in the fiber arm of the interferometer is equal to that in the air arm of the interferometer, thus the first term in the cosine function in the equation (27) is zero

$$\tau_{arm} - \tau_{fiber} = 0 = \frac{L_{air}}{c} - \frac{L_{fiber}}{c}\left(n' - \lambda'\frac{dn}{d\lambda}\right) \tag{28}$$

Where,

$$n_g(\lambda) = \left(n' - \lambda'\frac{dn}{d\lambda}\right) \tag{29}$$

At this center wavelength, the output intensity has the form shown below
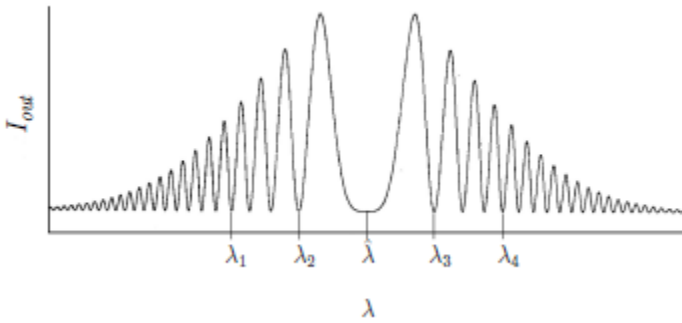
Figure 15: Spectrum of the output intensity at the center wavelength [11]

With such interferometric fringes in Figure 15 above, one can employ either direct or indirect techniques to obtain the second order dispersion coefficient and slope coefficients. These are discussed below [14].

Indirect Techniques

This involves changing the air-path length as the center wavelength changes. It is called an

indirect technique because it involves first relating different parameters in order to obtain the dispersion coefficient. For a shift in wavelength, the optical path difference changes, thus we use this information to determine the chromatic dispersion coefficient of the fiber. The following derivation shows how we arrive at the dispersion coefficient

Using the fact that at center wavelength, the propagation delay time of the fiber arm and the air arm are equal (from equation (28)), we have

$$\tau_{arm}(\lambda') = \tau_{fiber}(\lambda') = \frac{L_{air}}{c} + \frac{1}{c}\Delta L_{air} \tag{30}$$

But

$$D(\lambda') = \frac{1}{L_{fiber}}\frac{d\tau_{fiber}(\lambda')}{d\lambda'} \tag{31}$$

$$\Delta OPD = \frac{\tau_{fiber}}{c} \tag{32}$$

Thus chromatic dispersion coefficient is given as,

$$D(\lambda') = \frac{1}{L_{fiber}}\frac{\Delta OPD}{c\Delta\lambda'} \tag{33}$$

Direct techniques

This technique involves determining two wavelengths for example λ_1 and λ_2 of the output intensity minima on the same side of λ' as shown in Figure 15 above. However determining λ_1 and λ_2, involves first removing noise by smoothening the spectra and differentiating it. For minimum cosine function, we add $2m\pi$ to equation (27). We then substitute λ_1 and λ_2 to obtain two expressions of $I_{out}(\lambda_1)$ and $I_{out}(\lambda_2)$. Subtracting the arguments of the two expressions we arrive at the following equation:

$$\left[\frac{(\lambda_1-\lambda')^2}{\lambda_1} - \frac{(\lambda_2-\lambda')^2}{\lambda_2}\right]\frac{1}{2!}\frac{d^2n}{d\lambda^2} + \left[\frac{(\lambda_1-\lambda')^3}{\lambda_1} - \frac{(\lambda_2-\lambda')^3}{\lambda_2}\right]\frac{1}{3!}\frac{d^3n}{d\lambda^3} = \frac{2m\pi}{L_{fiber}} \tag{34}$$

However, only the first part of this equation contributes significantly to chromatic dispersion,

thus the second part of the equation can be neglected.

$$\left[\frac{(\lambda_1-\lambda')^2}{\lambda_1} - \frac{(\lambda_2-\lambda')^2}{\lambda_2}\right]\frac{1}{2!}\frac{d^2n}{d\lambda^2} = \frac{2m\pi}{L_{fiber}} \tag{35}$$

Where m is the number of intensity cycles of the output intensity separating λ_1 and λ_2 .

By substituting all the known parameters, $\frac{d^2n}{d\lambda^2}$ is obtained which is then substituted in equation (21) to obtain the chromatic dispersion coefficient D(λ).

Fourier Transform methods

This involves Fourier transforming the measured interferograms to obtain the chromatic dispersion. A broad band source is required and the intensity is measured over the whole wavelength region at once.

2.2.2 Modulation Phase Shift techniques (MPS)

MPS technique requires a tunable laser. The laser is intensity modulated and coupled into the fiber whose dispersion is to be measured as shown in the Figure 16, and then to the photodetector. The reference signal (from the electrical source) and the signal through the fiber under test are compared to determine the phase. The measurements are done over the whole wavelength range each time selecting a different wavelength from which the relative group delay is determined [15]. Then knowing the length of the fiber, chromatic dispersion coefficient is obtained from;-

$$D(\lambda) = \frac{1}{L}\left(\frac{\partial\tau}{\partial\lambda}\right) \tag{36}$$

Where L is the length of the fiber under test, τ is the relative group delay measured in ps and λ is the center wavelength measured in nm.
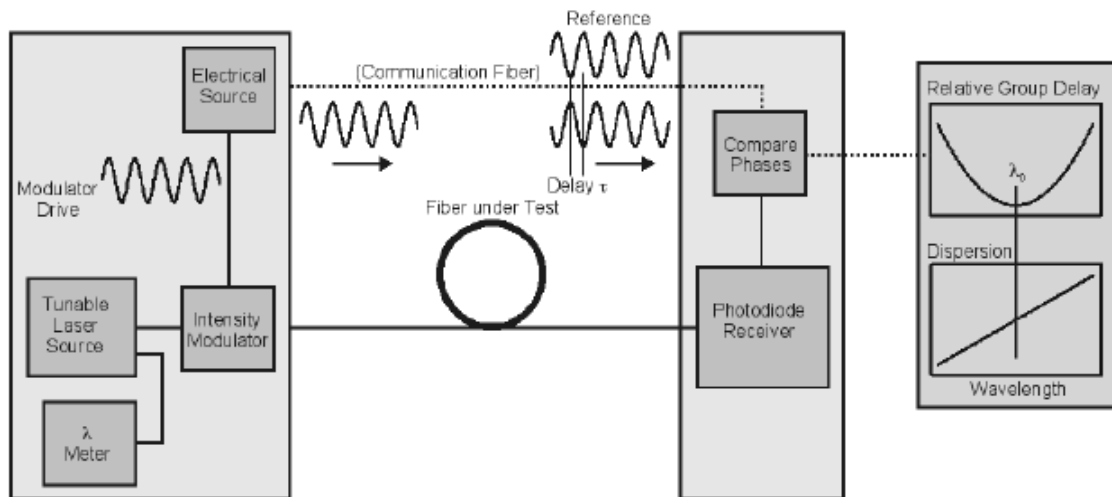
Figure 16: Schematic representation of the Modulated Phase Shift technique **[15]**

2.2.3 Time of Flight (TOF)

This method is common for long length fibers and the setup is shown in Figure 17. Fiber length of 100km can be measured with this method. Here four or more wavelength is coupled into the fiber under test using a pulse generator. Then the time delay for the pulses at each wavelength is determined and the relative group delay calculated from which the dispersion coefficient is obtained. Measurements can be done without connecting a reflective device at the other end of the fiber when the fiber termination is not an angled connector. The same equation as for the MPS technique is used here to calculate the dispersion coefficient [16].
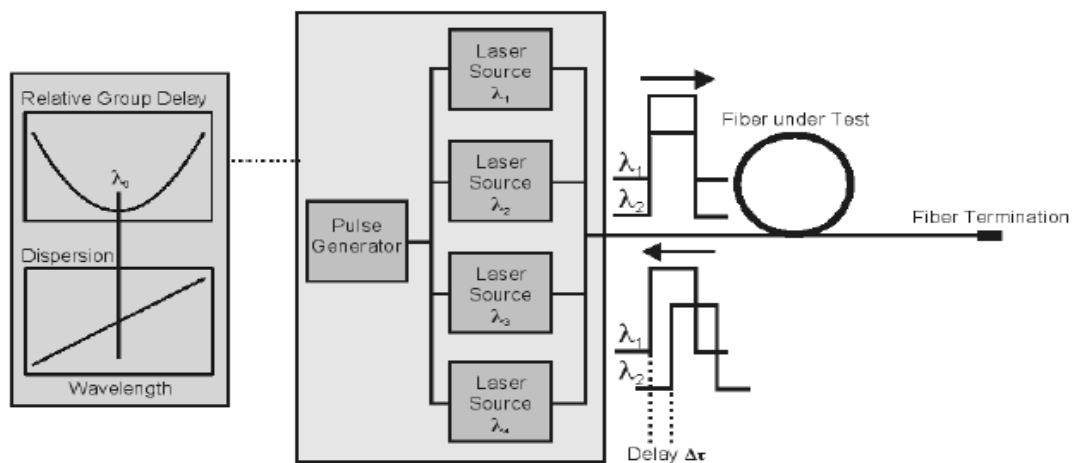
Figure 17: Schematic representation of Time Of Flight technique [16]

In both MPS and TOF techniques, curve fitting can help to improve precision of the results.

2.2.4 Comparison of the dispersion measurement techniques

In order to choose to choose an appropriate method for dispersion measurement, it is important first to compare and contrast the different methods.

In the Time Of Flight technique, the second-order dispersion parameter is determined by measuring the relative temporal delay between pulses at different wavelengths. Measurement precision achievable by the time of flight technique is on the order of 1 ps/nm [17]

For time-of-flight methods a source of narrow light pulses covering a wide spectral region is required. Discrete- wavelength laser diodes and broadband sources such as fiber Raman lasers, supercontinuum sources, or tunable soliton sources are commonly used for this. The output of such broadband sources can cover several hundreds of nanometers and even more [8].

In the Modulated Phase Shift technique[17], an optical signal is amplitude modulated by an RF signal and the dispersion parameter is determined by measuring the RF phase delay experienced by the optical carriers at the different wavelengths. Measurement precision achievable by the MPS technique is on the order of 0.07 ps/nm [19]

Modulated Phase Shift is being used as an industry standard method for measuring dispersion in optical fibers. However, it is expensive to implement and its precision is limited by both the stability and the filter in the RF signal [20]. Also both the Time of flight and the Modulated Phase Shift techniques require long lengths of fiber, from several tens of meters to several kilometers. Therefore, they are not desirable for characterizing specialty fibers or gain fibers, of which large fiber lengths are expensive to acquire or not available. Also, when fiber uniformity changes significantly along its length, the dispersion of a long span of fiber cannot be used to accurately represent that of a short section of fiber. In such cases, dispersion measurement performed directly on short fiber samples is desirable.

Four Wave Mixing involve the measurement of optical power in the generated idler wavelength. These techniques require the knowledge of zero dispersion wavelengths to extract the dispersion curve of the fiber [21|]. However, in fibers where no information is available on the zero dispersion wavelengths, or when laser sources are not available around zero dispersion

wavelength, this method becomes impractical [21]. The associated issue with the techniques relying on the measurement of power is the noise due to optical amplifiers. Even when filters are used, the measurement results are corrupted by the in-band noise [22].

Interferometric techniques, on the other hand, are capable of measuring dispersion on fibers of length below 1m [11]. Thus for the characterization of lengths around 1 m, it is preferable to utilize interferometric techniques [13]. Temporal interferometry [24] employs a broadband source and a variable optical path to produce a temporal interferogram between a fixed path through the test fiber and the variable path. The spectral amplitude and phase are then determined from the Fourier transform of the temporal interferogram. The dispersion is indirectly obtained by taking the derivative of the spectral phase. A precision of 0.0015 ps/nm measured on a 0.814m-long photonic crystal fiber [25] was recently reported using temporal interferometry. The main disadvantage of temporal interferometry is that it is susceptible to noise resulting from both translation inaccuracy and vibration of the optics in the variable path. A tracking laser is typically required to calibrate the delay path length [26, 27].

Spectral interferometry is generally more stable since the arms of the interferometer are kept stationary, and no tracking laser is necessary. It is often chosen for the dispersion characterization of photonic components [28-29] and depth-resolved optical imaging [30] such as optical coherence tomography (OCT).

In spectral interferometry, spectral fringes are produced by the interference of broadband light after propagating through two paths: one contains the test fiber and the other is a reference path containing a fixed delay. The spectral phase of the light wave passing through the test fiber relative to that through the reference path can be extracted from the fringe pattern, and in principle, higher order dispersion can be derived. Unbalanced techniques have the advantage of speed and simplicity, but they do not provide a direct measurement of the second-order dispersion. This means that curve fittings are required to extract second-order dispersion indirectly from the slope of the group delay (via numerical differentiation) [31] which may affect the accuracy of the results. In contrast, it is also possible to measure the second-order dispersion directly by employing a balanced dual-arm interferometer [32] with an adjustable optical path in one arm. The adjustable arm is adjusted to have the same group delay as the test fiber to remove the effect of the large linear dispersion in the interferogram. Their main disadvantage, however, results from the need for a variable delay line in the reference path. This makes measurements

very slow as every data point requires the acquisition of a separate spectral interferogram (SI) pattern.

It is thus clear that for short length fibers, even up to less than 1m, interferometric techniques are the best option. It is also a simpler method to conduct than other methods after the first adjustments have been made.

2.3 Dispersion compensation in data transmission systems

After dispersion measurements, control measures are taken to compensate for dispersion influence. This is however beyond the scope of this study. But one of the ideas how to improve the data transmission bitrate if the optical signal is rather far away from zero dispersion wavelength is to compensate for the accumulated dispersion optically by passing the (dispersed) pulses through specially designed fibers know as dispersion-compensating fibers characterized by a large negative total dispersion (Figure 18). For example if the central wavelength of the pulse is around 1550 nm, the red components of the pulse (i.e., longer wavelengths) will travel more slowly than the blue components (i.e., smaller wavelengths) of the pulse. Because of this, the pulse will be broadened. Now, after propagating through a G.652 fiber for a certain lengthL_1, the pulse is allowed to propagate through a length L_2 of a dispersion-compensating fiber (DCF), the red components (i.e., longer wavelengths) will now travel faster than the blue components and the pulse will tend to reshape itself into its original form. Indeed, if the lengths of the two fibers are L_1, and L_2 with dispersion coefficients D_1, and D_2 respectively, the pulse leaving the second fiber will be almost identical to the pulse entering the first fiber if [5]. Another idea is to alternate fibers with positive dispersion with negative dispersion elements (Figure 19) [6].

$$D_1 L_1 + D_2 L_2 = 0 \tag{37}$$
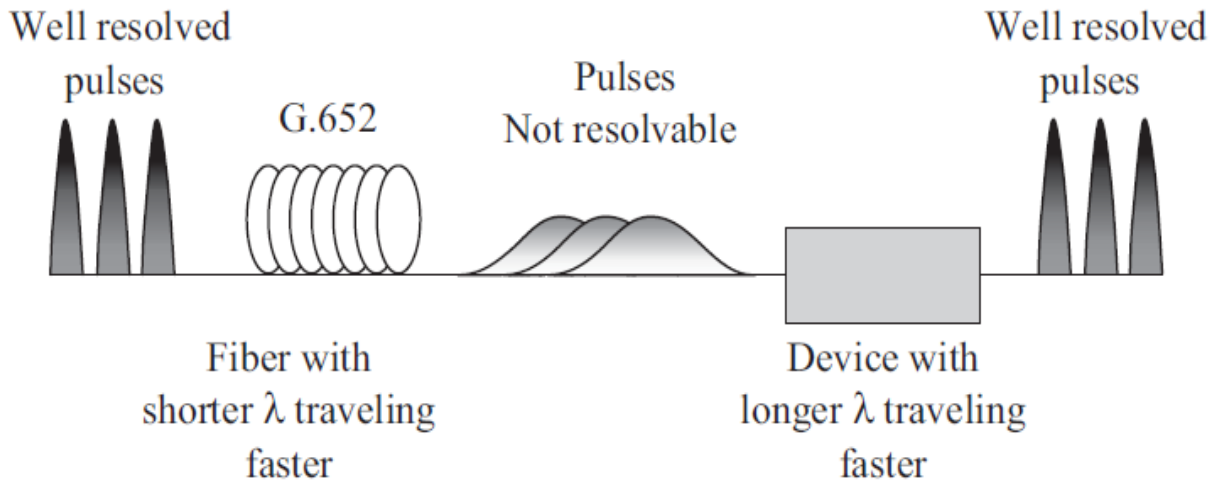
Figure 18: Concept of dispersion compensation. The link fiber is characterized by positive dispersion (i.e., longer wavelengths travel more slowly in the link fiber). The dispersion can be compensated by using a fiber in which longer wavelengths travel faster than shorter wavelengths [5].
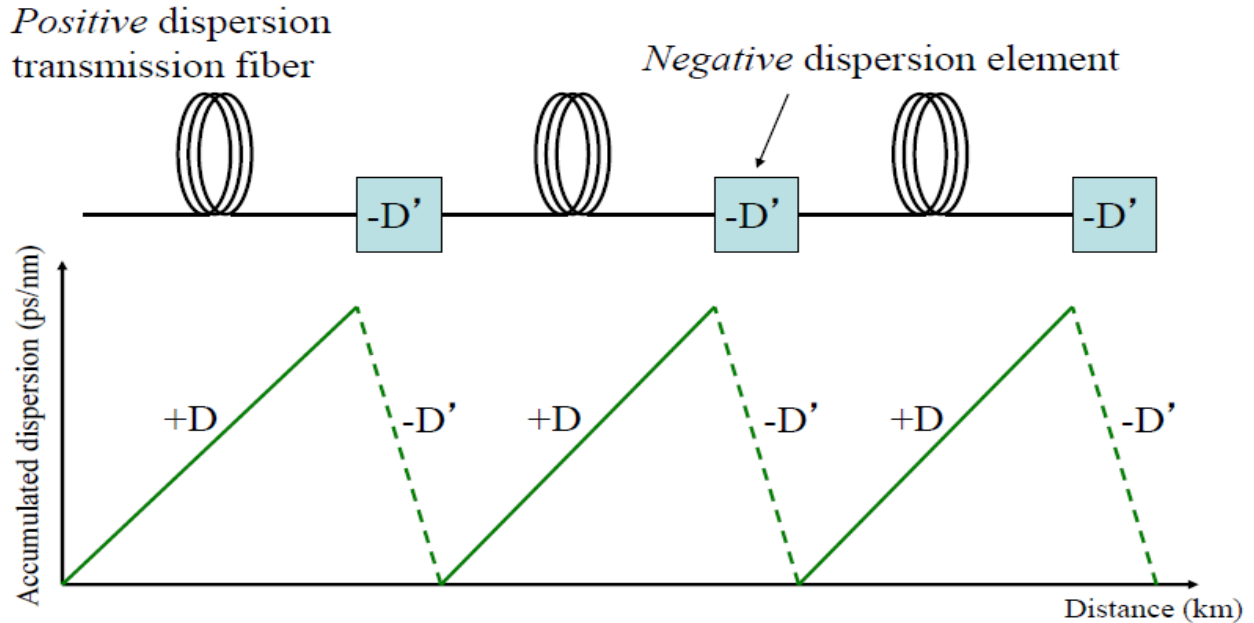
Figure 19: Dispersion compensation by altering fibers with positive dispersion with negative dispersion elements so that the total dispersion is zero at the end of the link [6]

Thus from the analysis in the previous sections it can be concluded that material dispersion is the

dominant dispersion mechanism in standard telecommunication fibers. Waveguide and Polarisation mode dispersion are weak and are sometimes ignored in the analysis. To maintain signal strength for a long distance, dispersion has to be measured and dispersion control measures taken especially for long distance transmission. For high quality and really ultra-short pulse fiber lasers, dispersion information is important for efficient generation and delivery of laser pulses.

2.4 ASE pumping source based on Tm^{3+}-doped fiber

In order to understand the functionalities of the source, it is important to understand the properties of such a source. An ASE source uses Tm^{3+}ion as the active ion in the fiber and detailed description of this ion is in the next section.

2.4.1 Tm^{3+} as a rare earth ion

Rare earth elements belong to the 6th row in the periodic table. They are also refered to as lanthanides. Their 4f shell is partially filled and sheilded from the external fields by the $5s^2$ and $5p^6$ electron shells. This makes the energy levels for this group of elements insesnsitive to the external environment. Due to the shileding of the 4f shell, the position of the energy levels in these elements is strongly influenced by spin-orbit coupling interractions than the applied crystal field. Because of this feature, luminiscence lifetimes for these ions are long and linewidths are comparatively narrow. These ions are capable of emitting over a wide range of wavelengths ranging from visible to infrared depending on the ion used. For the near infrared (1700-2000nm), Tm doped fiber is used with Tm^{3+} as the active ion. Figures 20 and 21 illustarate the energy levels of the rare earth ions labelling the most important radiative transitions.

The splitting of the energy levels in rare earth ions is due to stark splitting which broadens the energy levels due to applied crystal field despite the fact that the 4f shell is shielded and hence independent of the host.

2.4.2 Energy levels of Tm^{3+} ions

The angular momentum and spin quantum numbers of the rare earth ions are used during labelling. Sysmbols represent the total orbital angular momentum of the ion which is obtained by

combining the orbital angular momenta of the individual electrons in the ion using the Clebsch-Gordan series. The left and right subscripts represent the number of possible orientations of the total spin of the ion given by 2S+1 and the total angular momentum of the ion as determined by the Russell-Saunders coupling scheme respectively [33]. S is the total spin the ions.
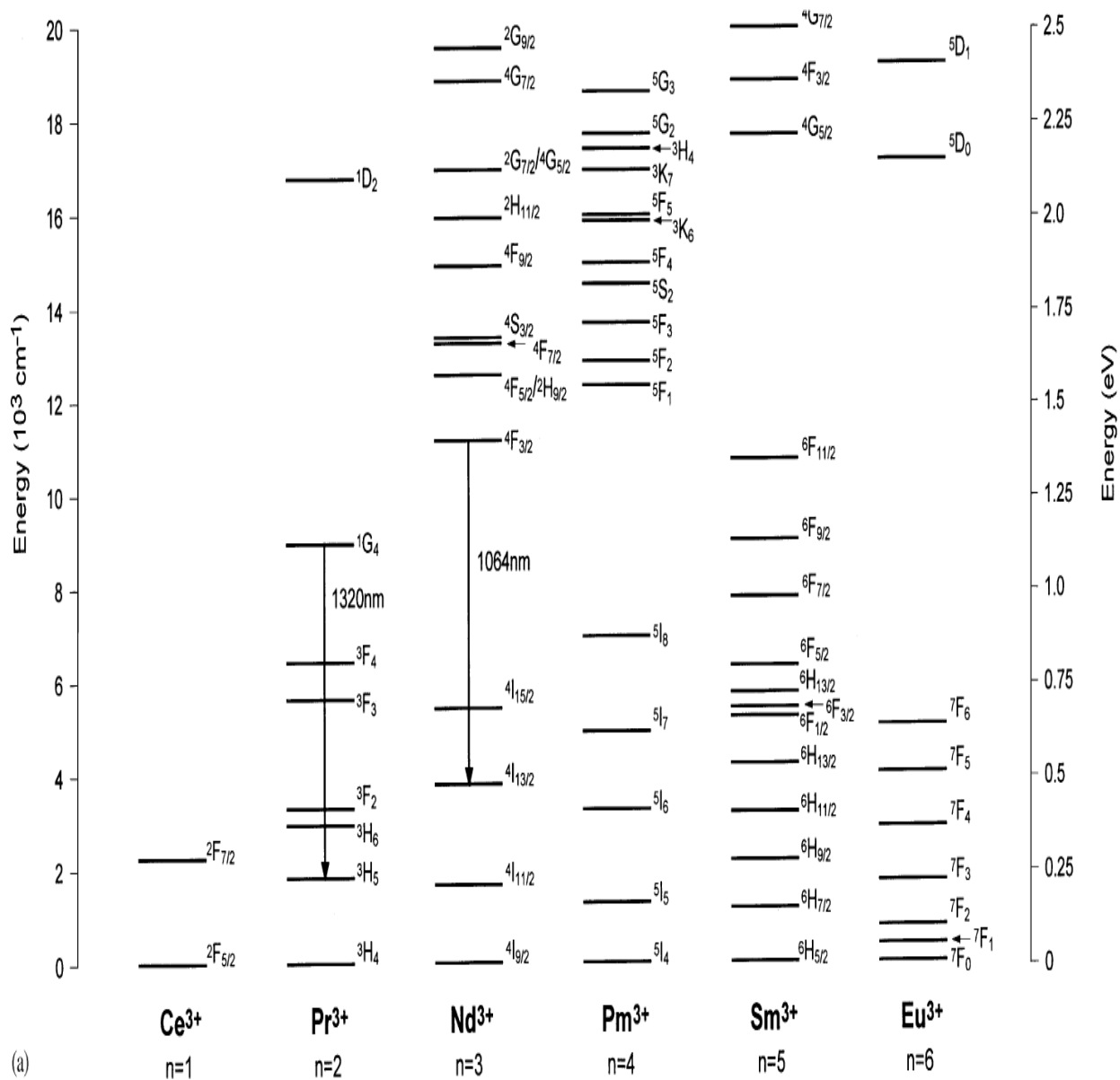
Figure 20: Energy levels of triply charged Lanthanide ions: The most important radiative transitions are labelled [34]
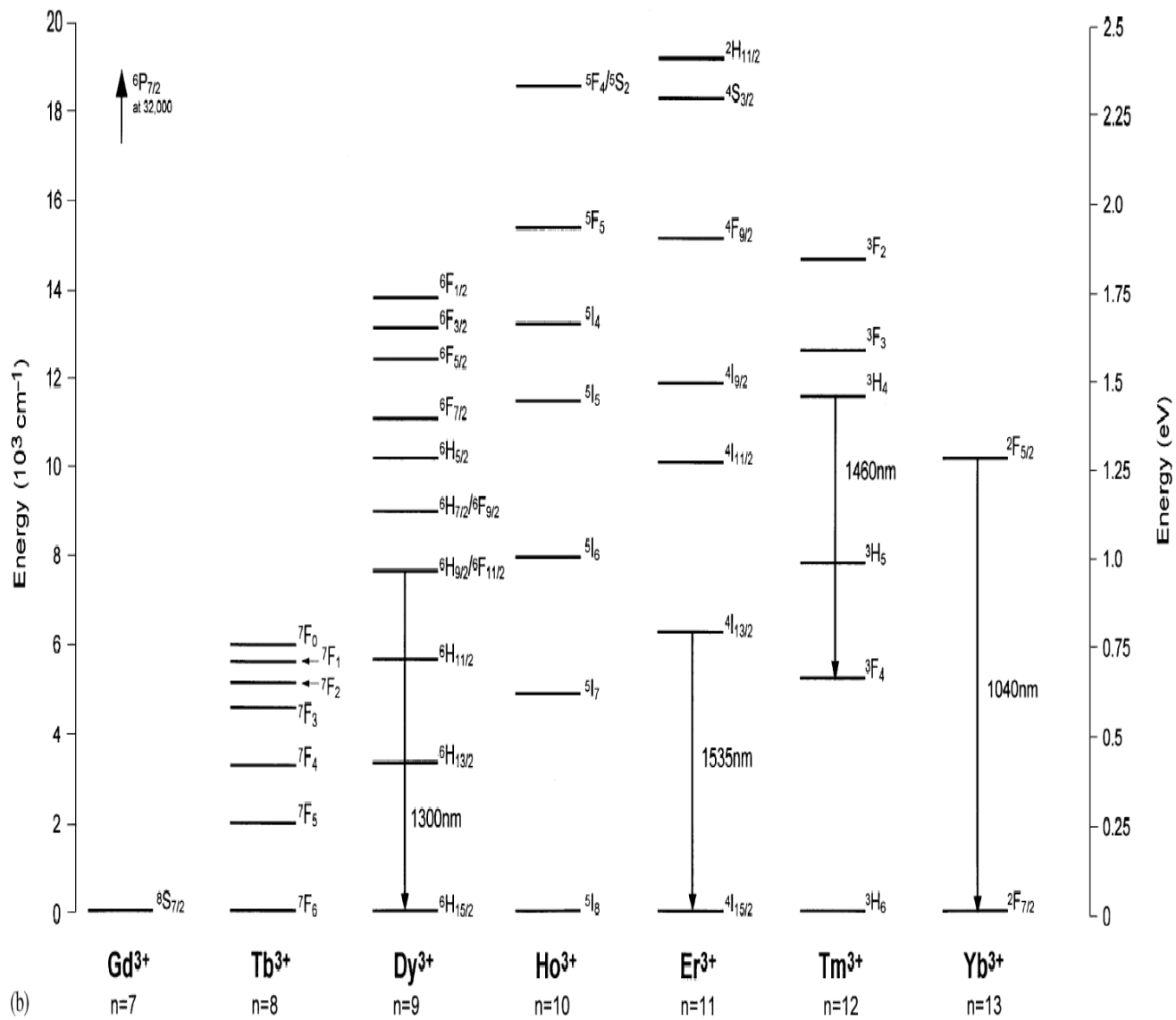
Figure 21: Energy levels of triply charged Lanthanide ions continued [34]
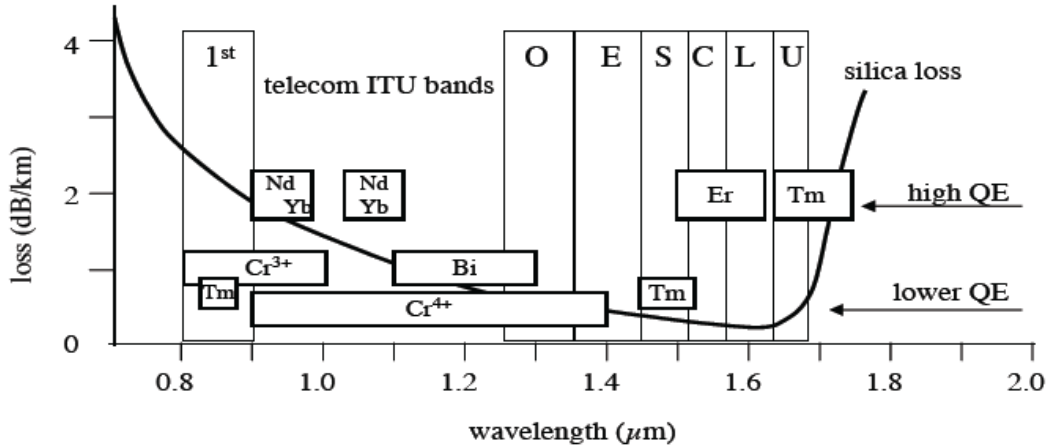
Figure 22: Wavelength ranges covered by standard dopants (rare-earth ions operating on high-QE transitions; top line) and alternative dopants (transition metal and rare earth ions operating on lower-QE transitions; bottom line) in silica- based fibers [35].

Thulium ion has three emission bands, at 820nm, 1470nm, and 1900nm. The 820nm and the 1470nm originate from the same $^3H_4$ energy level which suffers strong multi-phonon non-radiative (MP-NR) decay. MP-NR relaxations give low quantum efficiency (QE) and gain quenching due to bottlenecking effect on the lowest energy level of emission transition. Non-radiative decay is due to:-

1) High material phonon energy combined with a relatively small energy gap between the dopant emitting energy level and the level just underneath.

2) A strong electron-phonon coupling to the material which is due to site symmetry distortion imposed to the dopant as this is typical for transition metals. Typically silica has high phonon energy ($1100cm^{-1}$) compared to fluorides ($550cm^{-1}$) and offers distorted dopant sites.

Using the strong $^3F_4$ to $^3H_4$ emission band, we can obtain laser emission around 2µm. This however involves ASE filtering and gain flattening.

2.4.3 Thulium doped fiber lasers

Thulium (Tm) doped fiber lasers which operate in the near infrared region (1700-2100nm) truly revolutionized the high power laser technology [36]. This laser is considered to be with in the

eye safe wavelength range and thus, more attractive than Yb- Fiber lasers operating at 1µm for industrial and military applications.

Power scaling with this fiber laser is being achieved with peak powers now greater than 100kW without requiring complicated fiber designs or sacrificing beam quality [37]. Previously, fiber laser research was performed predominantly on Ytterbium (Yb)- doped fibers at 1µm. Yb-fiber lasers have been particularly successful because this materials system has a low quantum defect and there are many high brightness diode laser pump sources at 915-975nm to pump this type of fiber. These advantages have thus led to high efficiency operation of these laser systems. As a result, Yb-doped fiber lasers have been scaled now to powers above 3000W with close to diffraction limited beam quality [38]

Ytterbium- sensitized Erbium (Er:Yb) fibers operating at 1.55µm are also good for eye safe operation and there is abundance of fiber components and instruments with in this wavelength region which were primarily for telecommunications industry. However, power scaling for this fiber laser is limited by the back conversion effect [39].

Figure 23 shows the comparison of Yb-doped lasers at 1µm, Er:Yb- doped fibers at 1.5µm and Tm-doped fiber laser at 2µm. I notice that the power scaling of Tm-doped fiber lasers is rapidly developing and it has outperformed the Er:Yb fiber laser Technology[40]
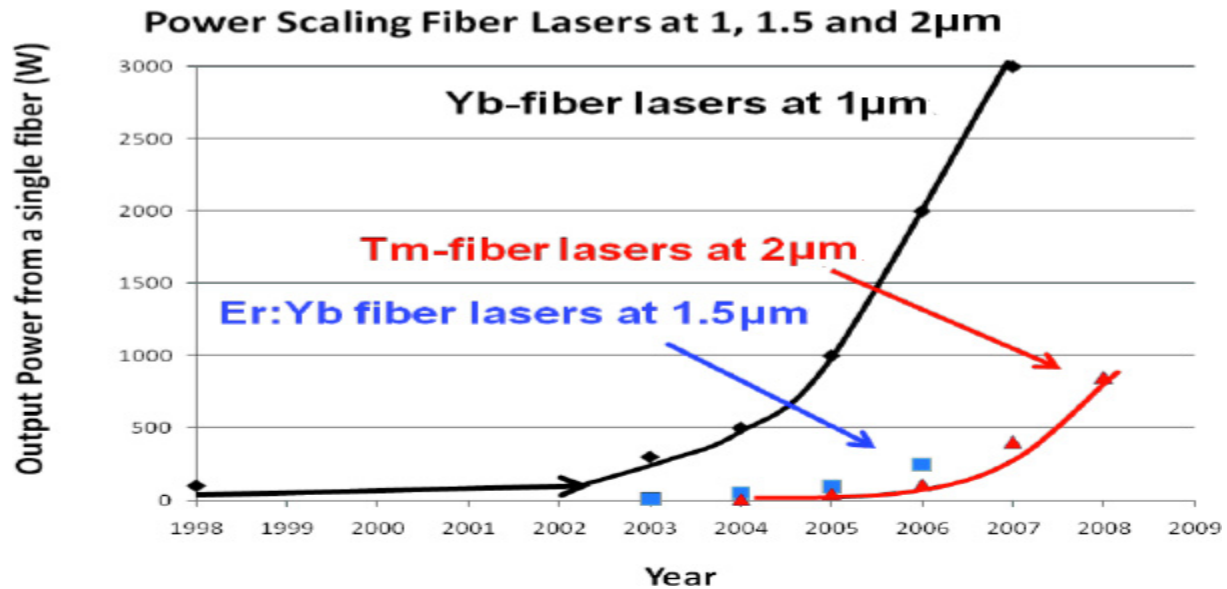
Figure 23: Comparison of power scaling for Yb-doped lasers at 1µm, Er:Yb- doped fibers at 1.5µm and Tm-doped fiber laser at 2µm. Improvements for Tm-doped fiber laser are more recent[40]

Tm can be pumped at two main pump bands: around 800nm and 1600nm. Pumping at 1600nm can be achieved by using forexample an Yb, Er –doped fiber laser since laser diodes at 1600nm are still relatively new. This attributes to the reduction in the overall optical efficiency of the system due to low efficiency of Er:Yb fiber laser [41]. The 800nm laser pump diodes are readily available for pumping the Tm.

Ideally due to lower quantum defect when pumping with 1600nm, it should yield high conversion efficiency than pumping at 800nm. However this is not true due to cross relaxation (or two for one) phenomenon which occurs when adjacent Tm ions are excited, it turns out that pumping at 800nm yields similar efficiency of 60-65% [39].
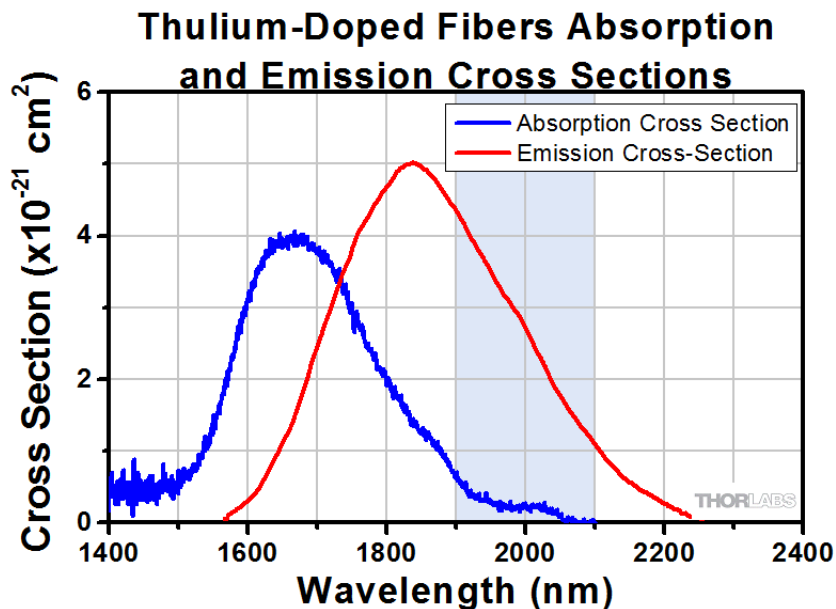
Figure 24: Thulium doped silica fiber laser emission and absorption cross-section [42]

2.4.4 Mid-IR Cr:ZnS laser

This is a broadband femtosecond solid-state laser. It is used in the dispersion measurement experiment in the 2150-2450nm wavelength region. The laser produces 1W average output power and pulse durations of about 70 fs with 5.6 nJ pulse energy [43]

33
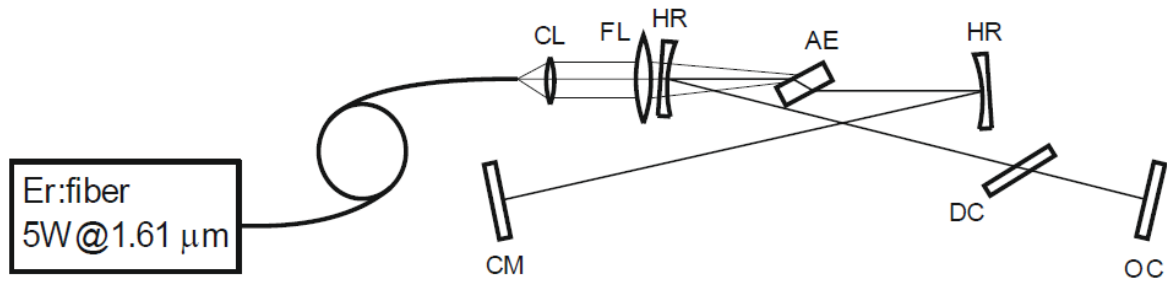
Figure 25: Schematic representation of femtosecond Cr:ZnS KLM laser [43]
CL-collimating lens, FL-focusing lens, HR-high reflecting mirror, AE-Cr:ZnS active element,
CM-chirped mirror, DC-dispersion compensation, OC-output coupler

The laser is pumped with CW Er-fiber laser which provides up to 5W output power at 1610nm (Figure 25). The beam from the laser is focused on to the active crystal by the AR-coated focusing lens. The cavity consists of two concave high reflecting mirrors, a plane reflector high chirped mirror (CM) and plane output coupler which has transmission efficiency of 18% at the laser wavelength. For mode locking, the soft aperture Kerr-lens effect with a moving chirped mirror is used.
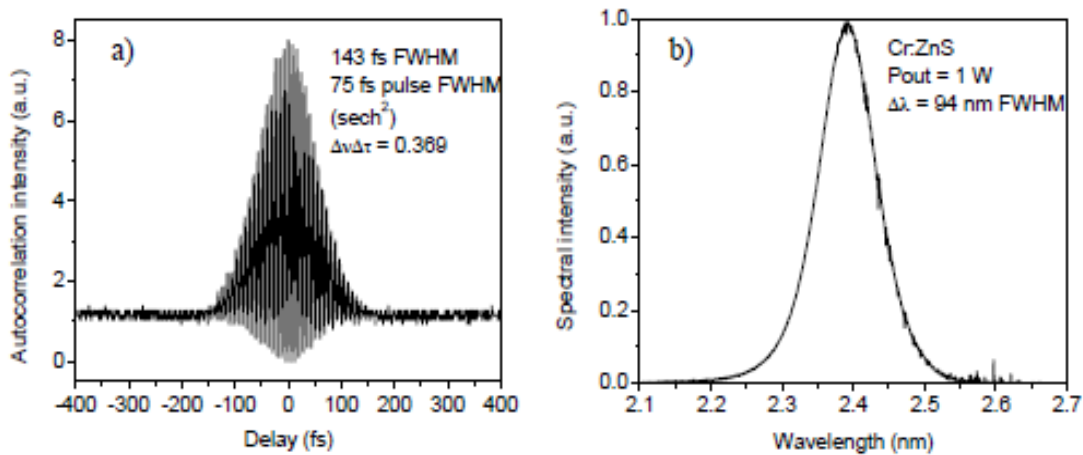
Figure 26: Interferometric autocorrelation trace (a) and optical spectrum (b) of KLM Cr:ZnS laser in harmonic mode locking mode producing an output power of 1W [43]

34

Thus from the previous discussions, a coherent source is the efficient pumping source for the experiment as we have less coupling losses into the fiber and especially a low coherent source because of short coherence length. Particularly a fiber laser is easy to design and requires no optical cavity as seen before and coupling from one fiber to another is easy and its temperature independent. For the 1W Cr:ZnS solid state laser, the coupling losses is not an issue since it's a high power laser because we can still obtain a high signal at the output.

Chapter Three: Methodology

3.0 Introduction

This chapter consists of the detailed setup description, automation process and the choice of components required for automation. Component selection is very vital especially by considering the measurement ranges and therefore by choosing the equipment for the specific range.

3.1 General scheme

The general experimental scheme (Figure 27) is based on the Mach Zhender interferometer as discussed in chapter two, section **2.2.1**. Basically light from a short coherence length source is split at the beam splitter into two beams. One beam is coupled into the fiber and the other goes through the air arm. They recombine at the beam combiner and then directed to the double prism Carl zeiss monochromator for spectral selection and an extended InGaAs photo-detector for detection. We investigate dependence of the change in the length of the reference arm required to equalize it with beam path in the sample arm on the wavelength.
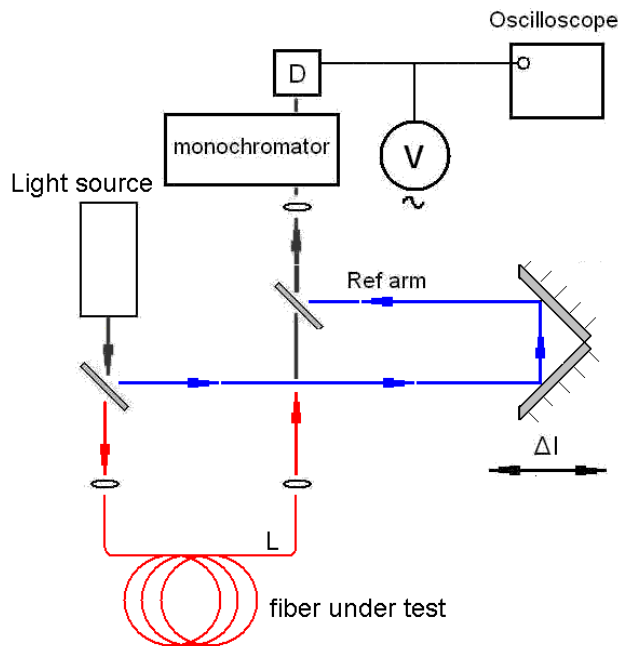
Figure 27: Schematic representation of the general dispersion measurement setup

3.2 How the dispersion measurement setup operates.

The dispersion measurement setup is shown in Figure 28. The beam from the source is split into two parts at the 50/50 beam splitter. One part is coupled into the fiber under test and the other part goes to the air arm (reference arm). An ordinary audio speaker with a glued mirror (M1) was placed in the reference arm for phase modulation of the fiber patch cord. The modulator was connected to the frequency generator operating at a frequency of about 300Hz [18].

The fiber arm signal and the reference arm signal later recombine at the beam combiner and then directed to the double prism monochromator for spectral selection and an extended InGaAs photo-detector for detection.
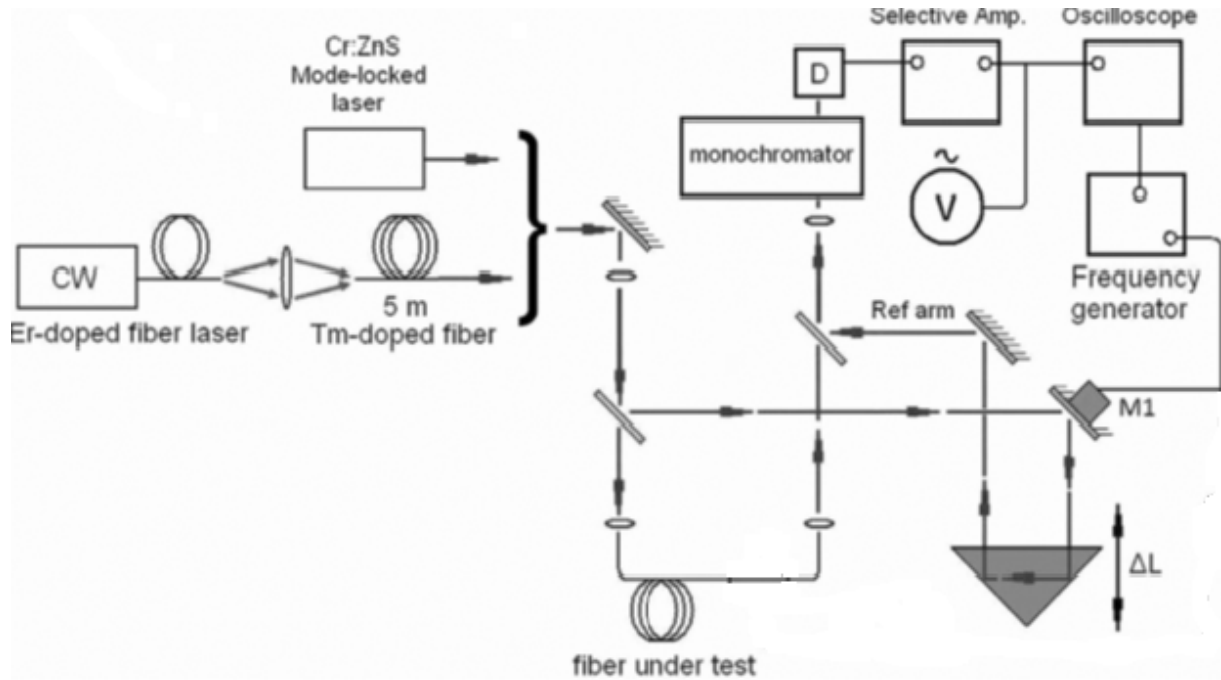
Figure 28: Experimental setup for dispersion measurements in short length fibers.

By using the refractive index of the test fiber and its length, the approximate arm position that corresponds to equal arm alignment was estimated. Then by using precise position controllers (step motor), the accurate position for equal arm alignment was determined. The dependence of the change in the length of the reference arm (Δl) required to equalize it with beam path in the sample arm on the wavelength was measured. Chromatic dispersion parameter D(λ), was then calculated from equation (45) derived in section **3.3**.

3.3 Determination of second order dispersion coefficient

To obtain the dispersion coefficient, different parameters are related as shown below.

If we consider the refractive index of the optical fiber being a function of wavelength, the group velocity is given by:

$$V_g = \frac{d\omega}{d\beta} \tag{38}$$

Where ω is angular frequency and β is propagation constant.

$$\beta = \frac{2\pi}{\lambda} n(\lambda), \qquad \omega = \frac{2\pi c}{\lambda} \tag{39}$$

Putting equation (39) in (38) we obtain

$$V_g = \frac{c}{n} / (1 - \frac{\lambda}{n}\frac{dn}{d\lambda}) \tag{40}$$

$where \qquad V_p = \frac{c}{n} \quad$ is the phase velocity

If the waveguide effect is neglected, the group delay (the transit time) for a light propagating in a fiber of length L is given by

$$\tau = \frac{L}{V_g} = \frac{Ln}{c}\left(1 - \frac{\lambda}{n}\frac{dn}{d\lambda}\right) \tag{41}$$

We can write the dispersion per unit fiber length is;

$$D = \frac{1}{L}\frac{\partial\tau}{\partial\lambda} \tag{42}$$

Differentiating equation (41) with respect to λ and then substituting it in equation (42) we obtain;

$$D = \frac{1}{L}\frac{\partial\tau}{\partial\lambda} = (-\frac{\lambda}{c})\frac{d^2n}{d\lambda^2} \tag{43}$$

Alternatively, the transit time can be given by

$$\tau = \frac{\Delta l}{c} \tag{44}$$

Putting equation (44) in (42) we get

$$D(\lambda) = \frac{1}{cL}\frac{d(\Delta l(\lambda))}{d\lambda} \tag{45}$$

Where $n, \lambda,$ c, and τ are the refractive index of the fiber, the wavelength, the velocity of light in free space and transit time respectively. Δl is the path difference required to equalize the two beams in the different arms.

Thus from equation (45), by measuring the paths length, Δl for different wavelengths, λ, the change in paths length, $d(\Delta l)$, corresponding to a given change in wavelength, $d\lambda$ are

determined. Then with the known lengths of the fiber, and the speed of light in the vacuum, the second order dispersion coefficient is calculated.

3.4 Signal sources for the experiment

Any experimental setup require signal source. The dispersion measurement setup used in this experiment is distinguished from the existing similar measurement systems [44], [45] because it uses new broadband light sources. These sources have been earlier described in chapter two. These sources are the Tm-doped fiber based source (ASE source) and a mode-locked femtosecond Cr:ZnS oscillator [46], [47].

An ASE made in the laboratory is used for the experiment in the near infrared region (1700nm-2000nm) and a femtosecond Cr:ZnS laser source from the NTNU laser physics group which can cover quite a broad spectrum from about 2150nm-2500nm is used in the mid-IR region. These sources are low coherent sources. Low coherent sources are good for this experimental setup because of their short coherence length which anables interference in quite a narrow region. It is thus easy to locate interference maximum with a high precision with such sources when the two lengths in the two signal paths are comparable. High coherent sources such as He-Ne laser have a long coherence length thus inteference occurs over a broad delay region, which reduces the precision of the equalisation of the interferometer arms.

3.4.1 Amplified Spontaneous Emission (ASE) source based on Thulium doped fiber.

ASE is a process where spontaneously emitted light (luminescence) is amplified. Spontaneous emission can be amplified to high levels especially in the laser medium with high gain and length (active fiber). Such light have low temporal coherence but rather high spatial coherence. The common way to generate ASE is the fiber laser cavity with low feed back operated below the laser threshold.

Considering the available laser sources on market for the mid-infrared applications such as the LEDs and semiconductor lasers, these have several problems such as high coupling losses when connecting them to fibers, high fabrication cost and their stability which relies on temperature which makes ASE sources a better option.

Preveously before lasers, incoherent sources (light bulbs) were being used but these were

insufficient due to high coupling losses. This is due to the fact that light from an incoherent source is emitted in all directions unlike for the laser that is targeted in one direction.

3.4.2 Why ASE source

ASE sources are able to provide a broad spectrum. Such sources are produced using the emission characteristics of the dopant ions in the glass host and the pumping wavelength. A pumping laser source is used to energise the dopant ions so that the spontanously emitted light from active ion propagates along the fiber, where it is amplified by the gain properties of the fiber, and finally emitted as an ASE. ASE source is advantageous over lasers in that it does not rely on optical feedback (no optical cavity is required). This makes the full-width at half maximum (FWHM) bandwidth of the backward ASE very broad [48].

Tm has a broad emission band which covers approximately 1700-2000nm which is almost a factor of 2 more than that of Erbium. Tm doped fiber laser sources have a variety of uses ranging from eye safe radar applications, Mid-IR generation applications such as spectroscopy, gas sensing, low coherence interferometer, excitation of biological and water based samples, industrial and medical applications. Its application for telecommunication has been limited due to high background loss of silica at 2000nm which requires a very appropriate transmission medium to overcome such losses. However, such transmission media are not available. The increasing internet traffic will require transmission applications in this wavelength region which will be made possible by such sources and further research in efficient transmission media in this wavelength region.

3.4.3 How to make an ASE source

For the ASE source, a high numerical aperture 5 m long Ge-doped Tm-co-doped fiber was pumped by the CW Er-doped fiber laser at 1.61 μm. The source produced a 300 nm broad (50 nm FHWM) superluminescent emission around 1.82 m. The optical power of ASE source is 5mW.The spectrum of this source is shown in Figure 29.
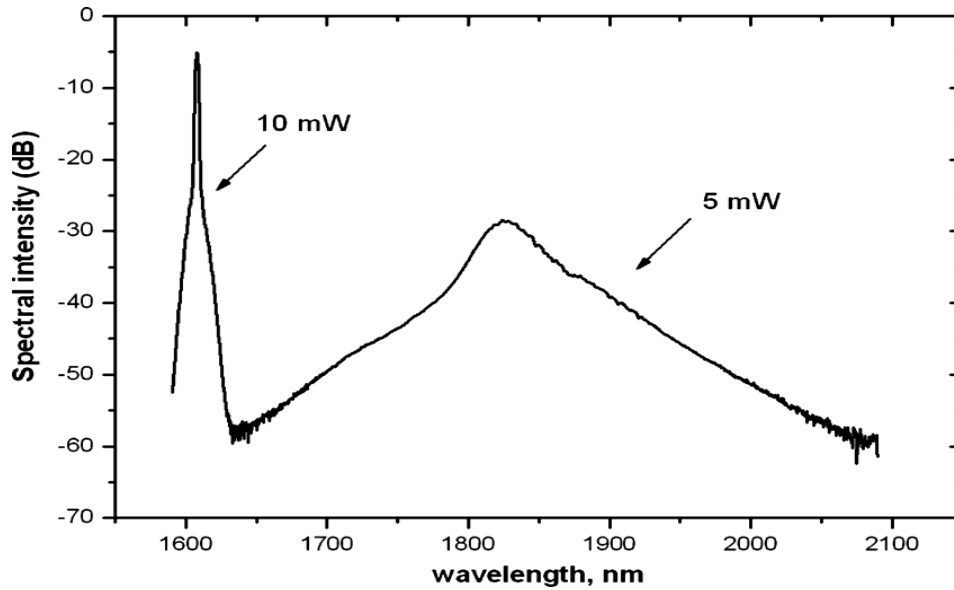
Figure 29: Spectrum of a broad band superluminescent Tm- doped fiber source used for pumping the experimental setup [18]

3.4.4 Mid-IR Cr:ZnS Laser

This laser was developed by my colleagues at NTNU laser physics research group. It produces 1W average output power at 20% optical efficiency. It generates about 70 fs pulses duration with pulse energy of 5.6nJ. The spectral width of this laser is over 100nm FWHM at 105-157 MHz repetition rates.

The spectrum of this laser is shown in Figure 30.
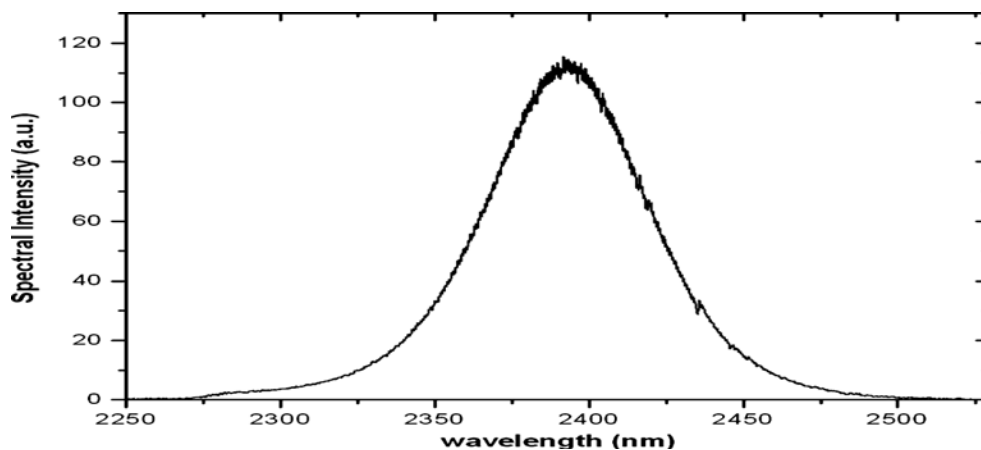
Figure 30: Emission spectrum of Cr:ZnS laser used for pumping the experimental setup. [18]

This light source exhibits low temporal coherence which allows achieving broad spectral coverage with the higher output power and with a high signal/noise ratio.

3.5 Choice of components

Precision is very vital for any instrument. Thus, components that are precise within the experimental measurement setup ranges are required. The selection criterion is described below.

3.5.1 Choice of the monochromator

A monochromator that can easily be automatized is required. Basically the one whose grating drive control can easily be integrated with a stepper motor is the best choice for this application. In addition, a grating with better resolution is required and the grating choice criterion is explained below.

Choice of the grating for the monochromator

Holographic gratings and ruled gratings are normally used. Holographic gratings are less efficient compared to ruled gratings. Thus holographic grating can be used for applications requiring low stray light or dense groove spacing while ruled gratings are for applications where efficiency and throughput of the optical system are very important. They are also suited for use in IR spectrum. Thus keeping all these advantages in mind, ruled gratings become a choice for this dispersion measurement setup.

Gratings are characterized by the grove density (the number of groves per mm on a grating surface) and a blaze wavelength (the wavelength at which the grating is at its maximum efficiency). The range of the grating can be estimated using the $\frac{2}{3}, \frac{3}{2}$ rule. This rule estimates the lower limit as $\frac{2}{3}$ of blaze wavelength and the upper limit as $\frac{3}{2}$ of blaze wavelength [49].

For this setup, the optimal choice would be a 1.6 µm blaze wavelength reflective diffraction grating (Figure 31) with the following parameters:-

Grooves (mm):   600

Blaze angle: 28^0 41'

Dispersion (nm/mrad): 1.46

Size (mm):   50x50
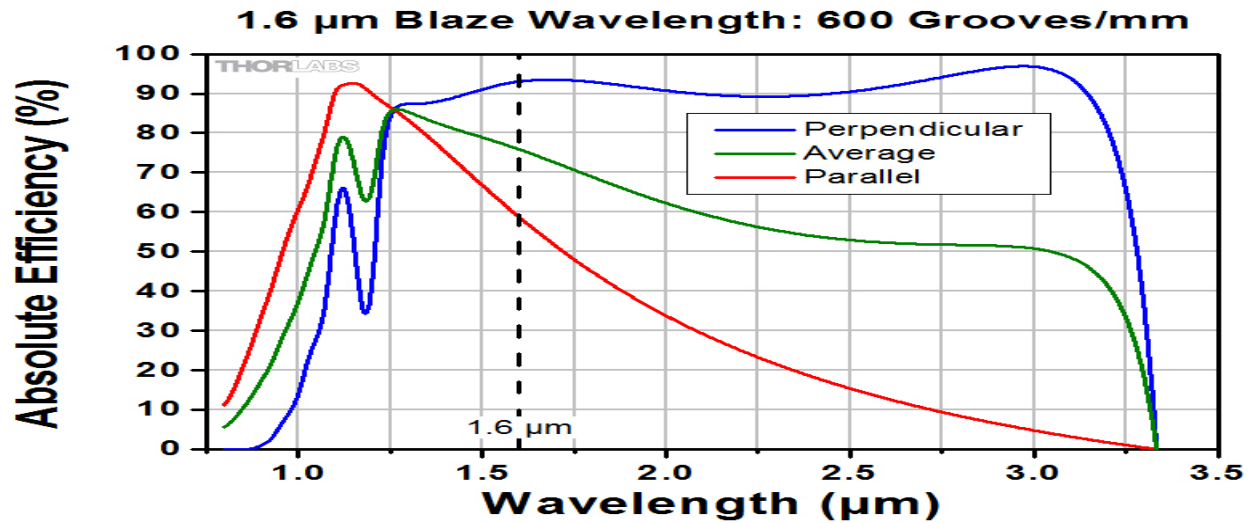
Figure 31: Efficiency curve of 1.6 µm blaze wavelength reflective diffraction grating [50]

3.5.2 Choice of the stepper motor

From the manual measurements, the translation stage moves about a distance of 2.5mm, for the whole interference range. Thus a stepper motor which moves approximately in the range 2.5mm to a few mm can be a good choice for this application. In addition a high precision stepper motor is required especially for really short fibers where precision is very vital. Typically a micro meter stepping motor is the best choice. Figure 32 shows the TRA12PPD stepper motor with its controller which were used in the experiment. The motor has the following parameters:-

Model: TRA12PPD

Travel range: 12mm

Maximum speed: 0.4mm/s

Minimum incremental motion: 0.1µm

Backlash: 10µm

43

Figure 32: TRA12PPD Miniature Stepper Motor Actuator with a stepper motor controller [51]

3.5.3 Conversion of analog signal to digital signal

The voltage signal from the detector has to be converted from analog into digital signal that is understood by the computer, thus an analog to digital converter is required. These converters are classified as: - stand-alone ADC,s and microprocessor compatible ADC's. Stand-alone ADCs often contain LCD or LED drivers and can be directly connected to a digital display. Usually, however, they cannot be connected to microprocessors or other digital circuits. When an ADC is used for process control or data acquisition systems where data must be fed to computers or dedicated microprocessor systems, it must be microprocessor compatible ADC. Thus microprocessor compatible ADC is the best choice for this application. The ADC used in the experiment is shown in Figure 33 and has the following parameters;-

Digital outputs: 4 channel, +5V pull-up

Analog inputs: 2 channels, $\pm 1V \pm 10V, 1V \ or \ 10V,$ programmable, 12-bit resolution, 50 Hz analog bandwidth

Figure 33: Conex IOD analog to digital converter/digital to analog converter [52]

3.6 Automation process of the setup

Generally automation is important because it increases throughput or productivity, improves quality or increases predictability of quality and improves robustness (consistency)

Automation process involves configuring the different components with appropriate devices and then synchronizing them together to have a complete automated setup. These include:-

1) Automation of the monochromator so that the wavelength , λ is automatically selected with an appropriate stepper motor

2) Using position controllers such as stepper motor to control the translation stage from which the paths difference, Δl can be determined.

3) Convert the analog signal from the detector into a digital signal that can be understood by the computer.

4) Relate the measurable parameters, λ, Δl and the maximum interference signal, V_{max} to calculate the dispersion parameter.

The schematic algorithm of the automation process is shown in Figure 34.
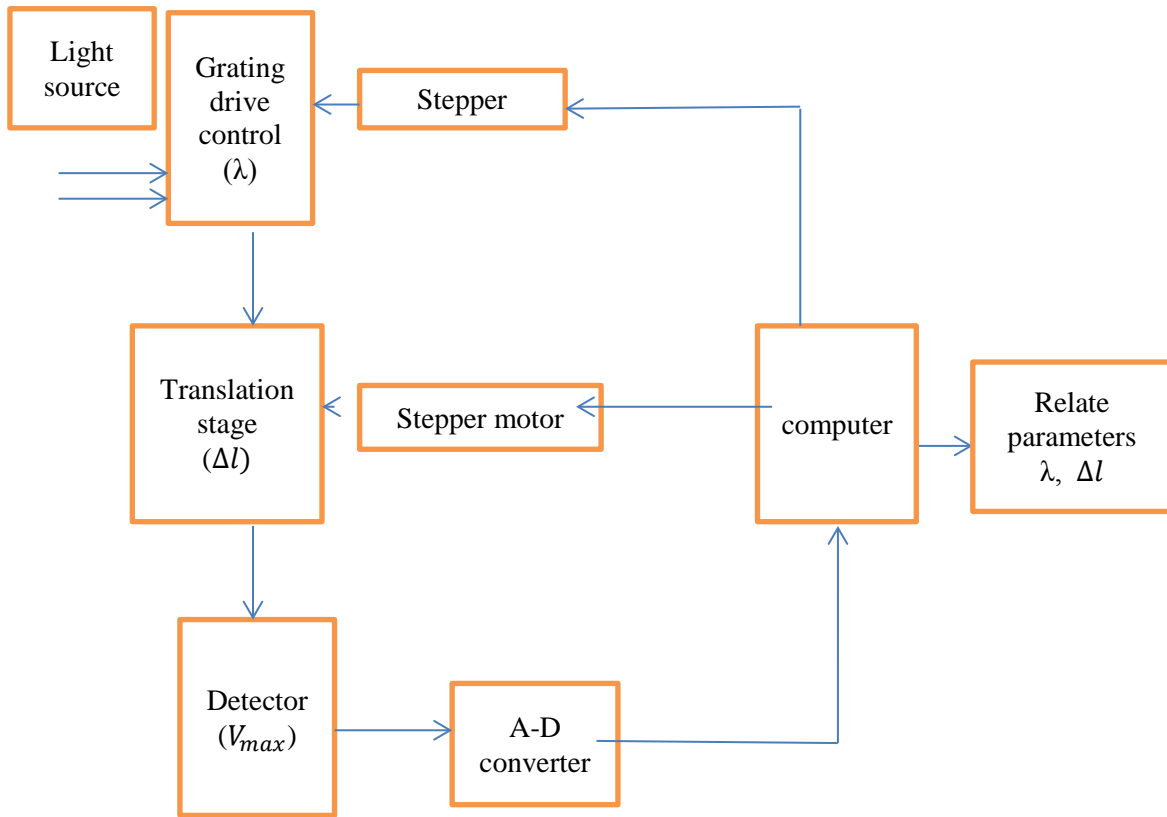
Figure 34: Schematic representation of the flow diagram

3.6.1 Automation of the monochromator

The mechanical part of the grating drive mechanism can be controlled by a stepper motor. This is because gratings disperse light by reflecting the wavelengths at different angles. Thus the angular position of the grating can be adjusted so that only the required wavelength of light is passed through the exist slit blocking other wavelength. Connection of a precision stepper motor to the rotary stage of the grating can help to achieve this. For high accuracy, a micro- stepping motor is required.

This part of automation was not fully realized in frames of the project due to lack of proper grating.

3.6.2 Automation of the translation stage

On the manual setup, one had to move the stage manually by adjusting the micrometer screw gauge attached to it. Automation of the translation stage involves the use of position controller to move the stage. Due to high sensitivity of the path difference for a slight change in λ, a high precision position stepper motor is used. For a given change in λ, from the automatized

monochromator, the stepper motor moves in response to wavelength λ in order to equalize the reference arm length with the length of the fiber under test.

The ADC is used to convert the analog signal from the detector into a digital signal that is conveyed to the computer. Thus digital signal is used as an input into the LabView based program to control the stepper motors.

3.6.3 Procedures for computer controlled setup

Labview software was used for programing. However it is also possible to program using other languages such as Fortran, C++, Visual Basic.

The translation stage moves using a stepper motor until the path length of the two arms are equalized. For each step that the motor on the translation stage moves, the current voltage and the previous voltage signals on the photodetector are compared until the maximum interference signal is obtained for a particular wavelength which corresponds to the maximum voltage signal from the photodetector. The analog voltage signal is converted to digital signal by the ADC from which we control the translation stage movement on the computer. The same procedure is repeated for the whole wavelength spectrum.

The motor first scans the whole interference spectral region from the edge to the end. It then steps back to the position corresponding to the maximum interference signal.

If V_n and V_{n+1} is the previous and the current voltage signals from the detector, a test condition is set which checks if $V_{n+1} < V_n$ for each step of the motor. The stepper motor on the translation stage continues to move in its subsequent steps until when $V_{n+1} < V_n$. The stepper motor then moves back to a step corresponding to V_n . This is the paths length required to equalize the two beams for a particular wavelength. The LabView front panel used for control of the setup is show in the Figure 35.
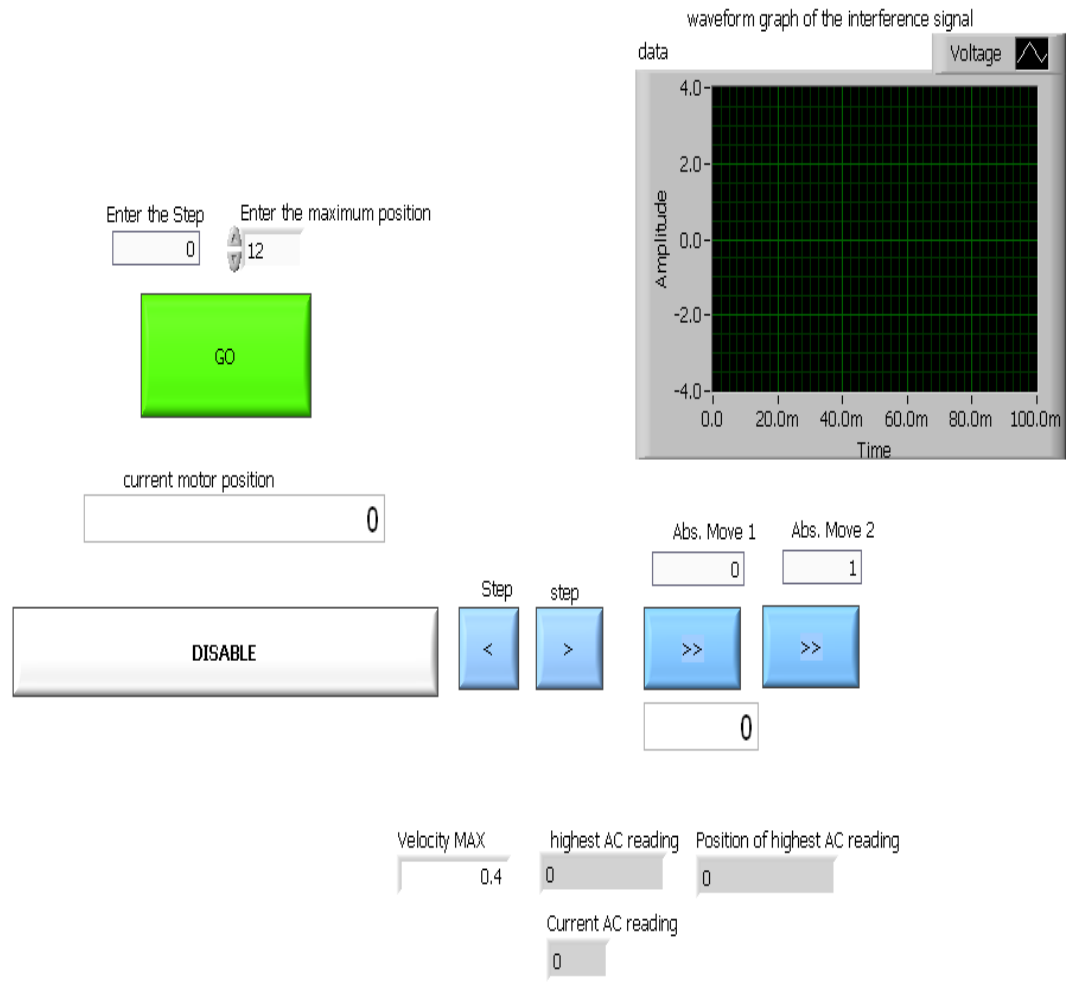
Figure 35: LabView front panel used to control the setup.

Chapter Four: Experimental Results

4.0 Introduction

For the dispersion setup test and calibration purposes, a silica fiber drawn at NTNU with similar composition to SMF-28 fiber was used. Both manual and automatic measurements were conducted for comparison purposes. Dispersion results were derived from equation (45) (i.e. $D(\lambda) = \frac{1}{cL}\frac{d(\Delta l(\lambda))}{d\lambda}$).

In addition, dispersion in other specialty fibers such as Ge-doped fiber, Yb:Tm doped fiber and Tm :Ge doped fiber was measured.

4.1 Dispersion measurement results for different fibers.

As discussed in chapter two, an indirect dispersion measurement technique was used, that is, dispersion coefficient is derived from other measured parameters. It is important to note that to obtain the change in path length for which the fiber arm and the air arms are equal, the position value of the translation stage is multiplied by a factor of two.

For two consecutive wavelengths, the change in wave length dλ, and the corresponding change in the paths difference dl, was determined. With the known length of the fiber, L, and speed of light in the vacuum, c, the dispersion coefficient was obtained from equation (45). A graph of dispersion coefficient against wavelength was then plotted. Tabulated dispersion coefficient values and the graphical dependence using manual and automatized setup for different specialty fibers are shown in the next sections.

The symbols used; - l1, l2, l3, ...correspond to the position of the motor for points of maximum interference signal, D-manual and D-auto correspond to manual and auto measured second order dispersion coefficients respectively.

4.1.1 Silica fiber drawn at NTNU.

This fiber was used for calibration of the setup and the length of the fiber used was $L = 75 \pm 0.05 cm$. In addition to testing different fiber length and comparison with theoretical data, different motor step sizes of 0.01mm and 0.001mm were also compared. The position of the step motor corresponding to maximum interference signal can be determined precisely with a smaller motor step size especially for short fibers (40cm-100cm) where the points of maxima are close to

one another. This was evident in Figure 37 as the result obtained with a 0.001mm step size was more accurate and a close approximate to the theoretical calculations than the 0.01mm step size result. Measurements were conducted in two wavelength ranges; - 1700nm-2000nm and 2150nm-2400nm.

The obtained dispersion results in silica fiber in the manual regime of the setup are given in the Table 3 including parameters that are used in equation (45) to obtain the dispersion results. These parameters include the position of the stepper motor l1 corresponding to a given maxima for a selected wavelength λ, and the change in paths length required to equalize the two arms dl1, for a change in wavelength dλ.

$\lambda \pm 2.5nm$	$l1 \pm 0.005mm$	dl1/mm	dλ/nm	dl1/dλ	D-manual(ps/nm.km)
1700	13.20	0.12	20	6000	27
1720	13.14	0.10	20	5000	22
1740	13.09	0.16	20	8000	35
1760	13.01	0.10	20	5000	22
1780	12.96	0.16	20	8000	35
1800	12.88	0.14	20	7000	31
1820	12.81	0.14	20	7000	31
1840	12.74	0.12	20	6000	27
1860	12.68	0.20	20	10000	44
1880	12.58	0.16	20	8000	36
1900	12.5	0.18	20	9000	40
1920	12.41	0.14	20	7000	31
1940	12.34	0.18	20	9000	39
1960	12.25	0.18	20	9000	40
1980	12.16	0.20	20	10000	44

Table 3: Dispersion in silica fiber drawn from NTNU in 1700nm-200nm wavelength range:- results obtained with Manual setup for length of the fiber, $L = 75 \pm 0.05cm$

The precision of the measured dispersion in the last column was based on the on the biggest uncertainty in the measurements which was from the selection of wavelength on the monochromator. Considering the minimum wavelength reading of 20nm, we estimate the uncertainty in the wavelength selection as $\pm 2.5nm$. For $\pm 2.5nm$ change in wavelength, there was a big change in the calculated dispersion value (all the significant figures changed) thus I rounded the dispersion value to the nearest full figure. The measured dispersion parameter in all the tables for all the measurements was based on the same criterion.

After changing the regime of the setup from manual to auto regime, measurements were done with the same fiber as the one used for manual measurements (similar fiber type and length). This was done in order to compare the results from both regimes. Table 4 shows the auto measured dispersion results in silica fiber drawn at NTNU with 0.01mm motor step size.

$\lambda \pm 2.5nm$	$l1 \pm 0.0001mm$	dl1 /mm	dλ/nm	dl1/dλ	D-auto(ps/nm.km)
1720	9.5792	0.0995	20	4976	22
1740	9.6496	0.1408	20	7042	31
1760	9.7285	0.1576	20	7884	35
1780	9.7784	0.0998	20	4992	22
1800	9.8383	0.1199	20	5997	27
1820	9.9281	0.1794	20	8974	40
1840	9.9880	0.1198	20	5991	27
1860	10.0694	0.1627	20	8136	36
1880	10.1481	0.1574	20	7870	35
1900	10.2198	0.1434	20	7170	32
1920	10.3079	0.1762	20	8810	39
1940	10.3880	0.1602	20	8010	35
1960	10.4596	0.1432	20	7160	31
1980	10.5894	0.2596	20	12980	57
2000	10.6598	0.1408	20	7040	31

Table 4: Dispersion in silica fiber drawn from NTNU in 1700nm-200nm wavelength range:- results obtained with computer controlled setup for L=75cm and with 0.01mm motor step size.

Dispersion results obtained in the manual regime and the auto regime were compared to check whether they are in agreement with each other. Both results were compared in reference to the theoretical calculation results for SMF 28 as shown in Figure 36. Results showed that they are in agreement with each other and also with the theoretical calculations. The slight difference could have been caused by the poor resolution of the monochromator used for wavelength selection. Also the composition of silica fiber drawn at NTNU could have been slightly different from SMF 28 used for theoretical calculations.
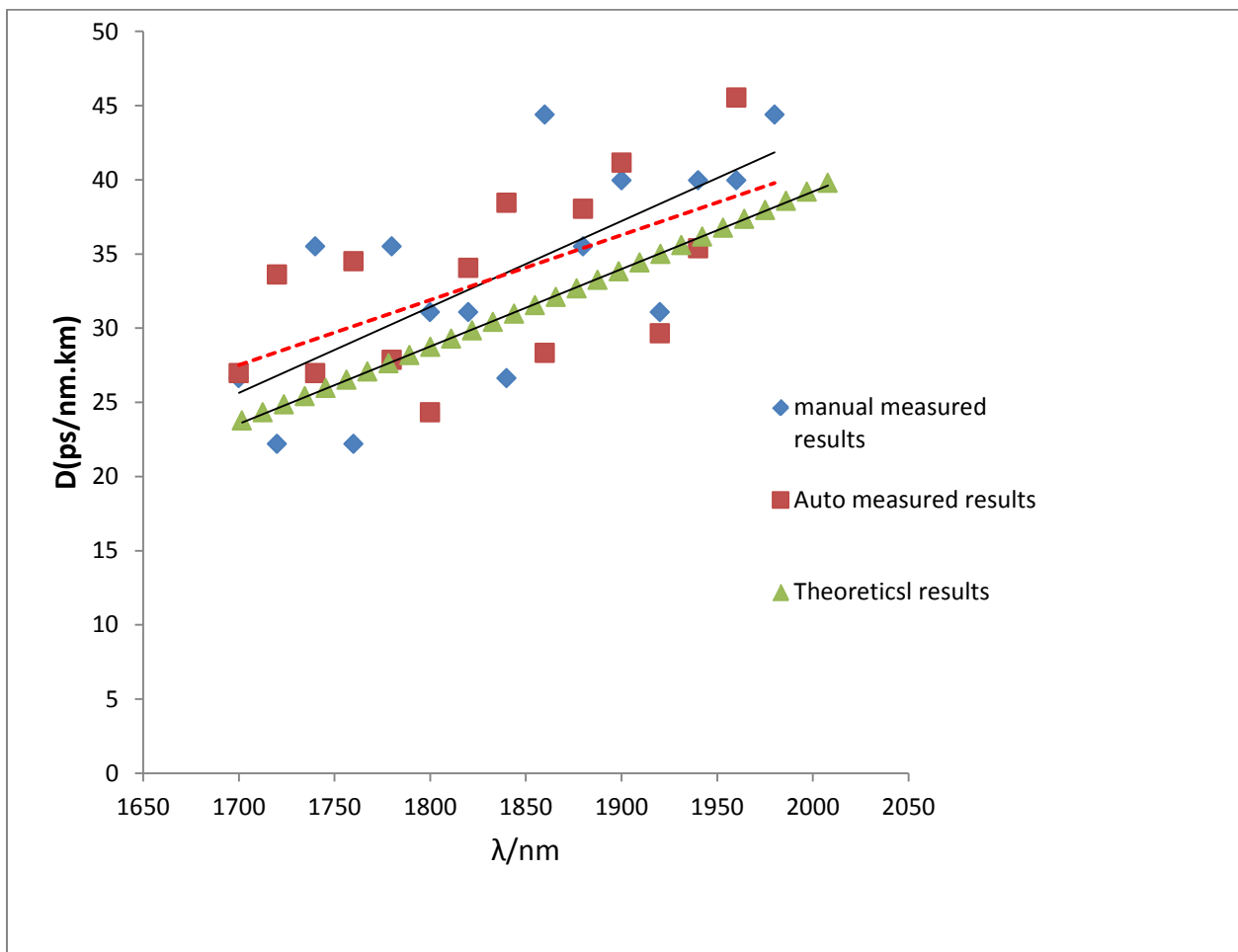
Figure 36: Comparison of manual and Auto-measured results with theoretical results in the 1700nm-2000nm wavelength range.

Table 5 shows the dispersion results in silica fiber drawn from NTNU for 0.01mm and 0.001mm motor step size. A clear comparison with the theoretical calculations can be seen in Figure 37.

$\lambda \pm 2.5 nm$	D-auto-0.01mm(ps/nm.km)	D-auto-0.001mm(ps/nm.km)
1720	22	27
1740	31	34
1760	35	27
1780	22	35
1800	27	28
1820	40	24
1840	27	34
1860	36	38
1880	35	28
1900	33	38
1920	39	41
1940	36	30
1960	32	35
1980	58	46

Table 5: Comparison of the computer controlled setup results in silica fiber drawn at NTNU for 0.01mm and 0.001mm motor step sizes in the 1700nm-2000nm wavelength range.

Figure 37 illustrates the dispersion results in silica fiber drawn from NTNU for 0.01mm and 0.001mm step sizes in comparison with the theoretical calculations. The 0.001mm and 0.01mm step size results are nearly in agreement with each other. This confirmed the repeatability of the results due to automation. The small difference is probably a result of low precision and repeatability in the selection of wavelength in the monochromator.
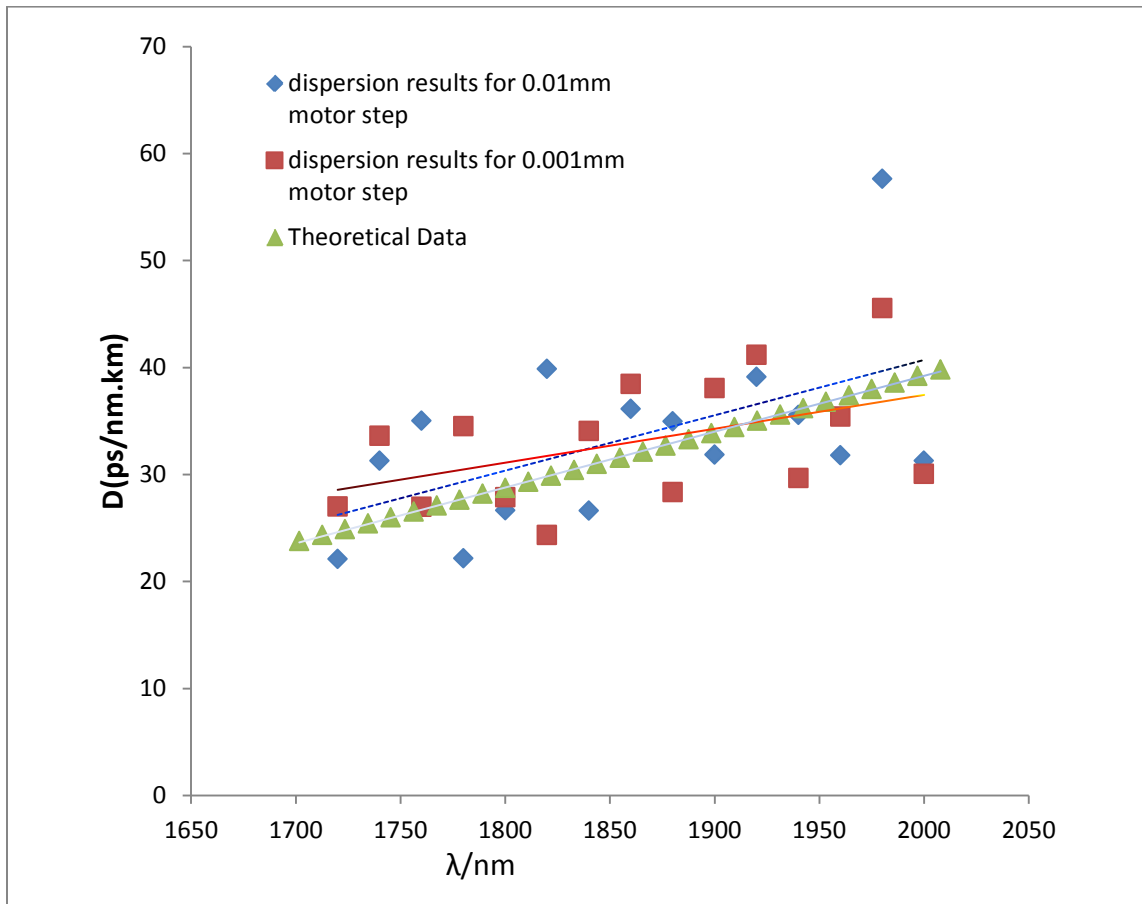
Figure 37: Comparison of dispersion in Silica fiber drawn from NTNU for different motor step sizes with the theoretical dispersion data in the 1700nm-2000nm wavelength range.

Table 6 shows the dispersion results obtained with two different fiber lengths. These measurements were done to test how precisely we could measure dispersion in shorter fibers. Results for fiber length of 207cm were compared with 75cm.

$\lambda \pm 2.5nm$	D-CrZnS/ps/km*nm (L=2.07m)	D-CrZnS/ps/km*nm (L=0.75m)
2230	48	44
2240	64	44
2250	64	106
2260	52	71
2270	58	44
2280	68	71
2290	74	89
2300	61	53
2310	61	36
2320	68	44
2330	81	53
2340	81	98
2350	87	62
2360	81	80
2370	87	80
2380	93	89
2390	90	98

Table 6: Comparison of dispersion results for length of the fiber, L=2.07m with L=0.75m in the 2150nm-2400nm wavelength range for Silica fiber drawn from NTNU.

Figure 38 shows dispersion in silica fiber drawn at NTNU for fiber length of 207cm and 75cm. The results for fiber length of 75cm were more noisy in comparison to the results for fiber length of 207cm. The short fiber length results in the small change in the length of the reference arm, dl for the neighboring wavelength and thus increases the influence of the position detection uncertainty of the measurements.
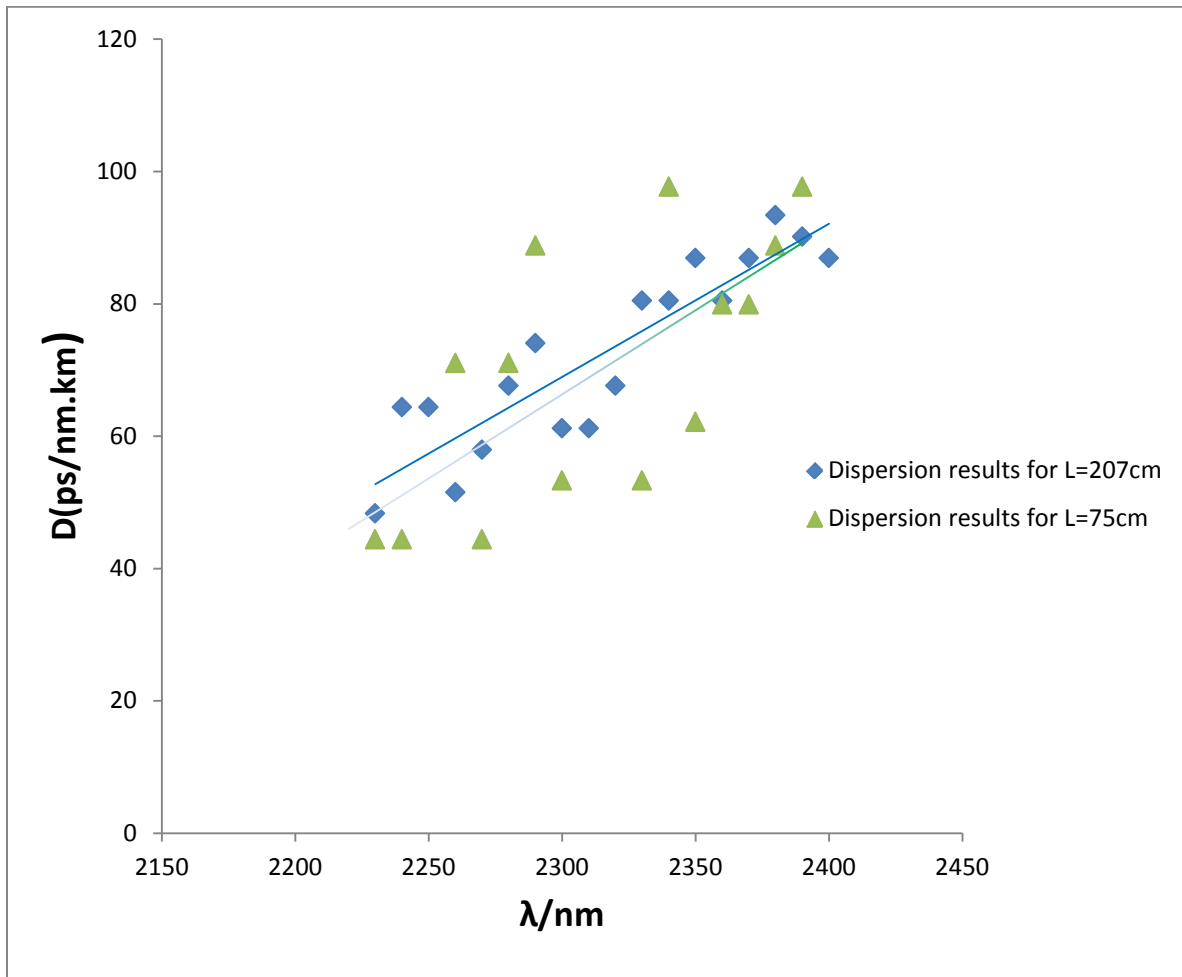
Figure 38: Comparison of dispersion results in Silica fiber drawn at NTNU for fiber length of 207cm and 75cm in the 2150nm-2400nm wavelength range.

By combining the results obtained in the two wavelength ranges measured using the two different pumping sources (1700nm-200nm and 2150nm-2400nm wavelength regimes), the dispersion trend from 1700nm-2400nm was obtained as illustrated in Figure 39.

Silica fiber drawn at NTNU exhibits positive dispersion in this wavelength range and its dispersion is seen to increase with increasing wavelength. This is typical characteristic of SMF 28. The results in the 2150nm-2400nm wavelength range were noisy in comparison with the results in the 1700nm-2000nm wavelength range, because the coherence length of Cr:ZnS laser was much longer than that of Tm-fiber superluminescent source. As a result, the interference maxima were broader for a particular wavelength for this laser source, thus complicating the detection of the center wavelength. Better results require re-adjusting of the Cr:ZnS laser for shorter pulse generation which was not part of my task.
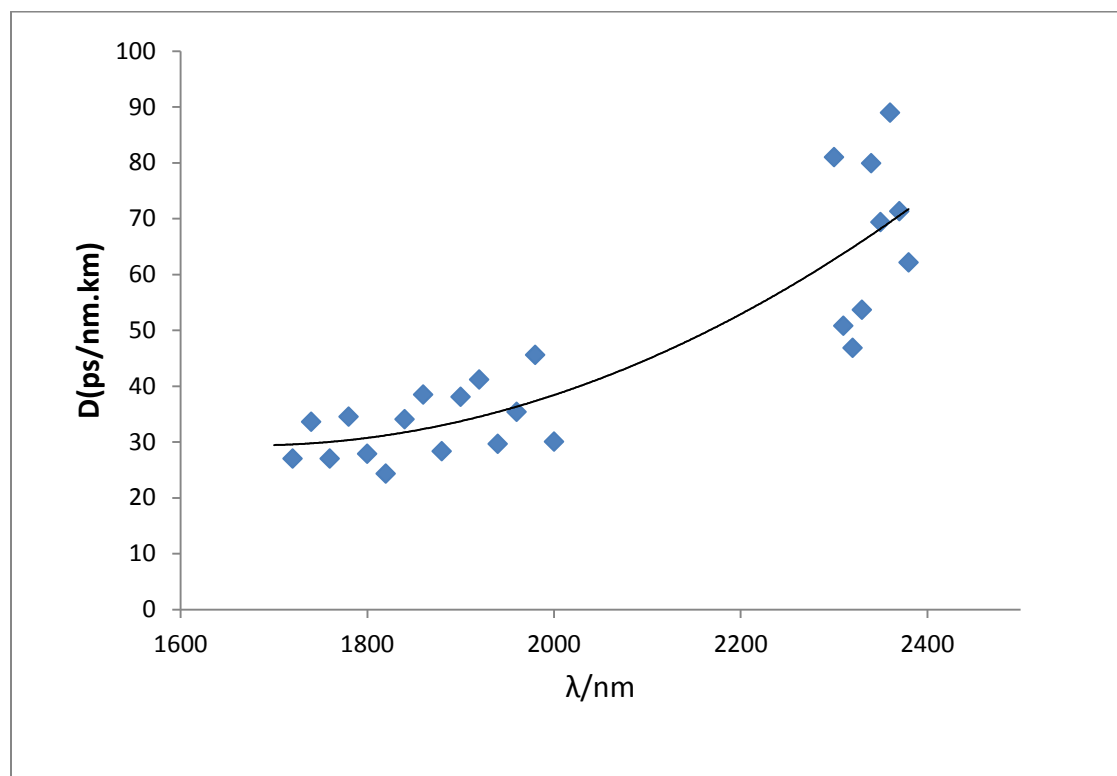
Figure 39: Dispersion distribution in silica fiber drawn from NTNU in the 1700nm -2400nm for fiber length L=75cm.

4.1.2 Ge-doped fiber

The length of Ge-doped fiber used for measurements in the experiment was $70 \pm 0.05cm$. There were several observed maxima interference points for each particular wavelength in Ge-doped fiber. The fiber exhibits waveguiding not only in the core but also in the cladding, and due to small core diameter (about 3µm) and unoptimized coupling, some light was coupled into the cladding. The multi-maxima interference behavior is a result of mixing of the core modes with the cladding ones. Approximately seven maxima were observed in the 1700nm-2400nm wavelength range as shown in the Table 7.

λ ± 2.5nm	l1 ± 0.0001mm	l2 ± 0.0001mm	l3 ± 0.0001mm	l4 ± 0.0001mm	l5 ± 0.0001mm	l6 ± 0.0001mm	l7 ± 0.0001mm
1700	16.5010	16.4101	16.3302	16.2402			
1720	16.4201	16.3303	16.2402	16.1603	16.0704		
1740	16.2502	16.1503	16.0704	15.9805	15.8906		
1760	16.0704	15.9905	15.9006	15.8107	15.7208		
1780	15.9805	15.8806	15.7907	15.7208	15.6309		
1800	15.9106	15.8207	15.7308	15.6408	15.5509	15.4710	15.3411
1820	15.8406	15.7507	15.6508	15.5768	15.4701	15.3611	15.2612
1840	15.8207	15.4910	15.3811	15.2812	15.2113	15.1114	15.0214
1860	15.6209	15.3911	15.2912	15.2013	15.1213	15.0314	14.8616
1880	15.4710	15.2912	15.2412	15.1413	15.0414	14.9415	14.8716
1900	15.3012	15.2412	15.1413	15.0514	14.9415	14.8616	14.7717
1920	15.0503	14.9604	14.9600	14.8805	14.7606	14.6707	14.5668
1940	14.8801	14.7802	14.7003	14.6004	14.5005		
1960	14.7802	14.7103	14.6204	14.5205	14.4106		

Table 7: Paths length for different modes observed in Ge doped fiber due to core and cladding coupled modes in the 1700nm-2000nm wavelength range.

By plotting the points of maxima in Table 7, we obtain Figure 40 which shows that these points of maxima correspond to different modes propagating through the fiber. It was how however hard to identify the core mode from all the observed modes. I therefore obtained an approximate of the total dispersion of both the core and cladding modes by averaging all the modes.

Figure 40: Path lengths for different modes propagating through the Ge-doped fiber in the 1700nm-2000nm wavelength range.

Table 8 shows an estimate of core and cladding dispersion obtained by averaging the core and cladding coupled mode results in table 7.

$\lambda \pm 2.5nm$	$l1 \pm 0.0003mm$	dλ/nm	dl1/mm	dl1/dλ	D/ps/nm.km
1700	16.3710	20			
1720	16.2441	20	-0.25173	-12586.5	-60
1740	16.0684	20	-0.35172	-17586	-84
1760	15.8982	20	-0.3396	-16980	-81
1780	15.8010	20	-0.1958	-9790	-47
1800	15.6375	20	-0.32543	-16271.4	-77
1820	15.5589	20	-0.1582	-7910	-38
1840	15.3314	20	-0.45546	-22772.9	-108
1860	15.2160	20	-0.22837	-11418.6	-54
1880	15.1421	20	-0.14846	-7422.86	-35
1900	15.0446	20	-0.19694	-9847.14	-46
1920	14.8352	20	-0.41731	-20865.7	-99
1940	14.6924	20	-0.28663	-14331.4	-68
1960	14.6080	20	-0.1678	-8390	-40

Table 8: Dispersion parameters for the averaged maxima (modes) observed in Ge doped fiber in the 1700nm-2000nm wavelength range.

Figure 41 shows the estimated core and cladding mode dispersion in 1700nm-2000nm wavelength range in Ge-doped fiber obtained by averaging both the core and the cladding coupled modes. From this graph, it was observed that Ge-doped fiber exhibits negative dispersion in this wavelength region.
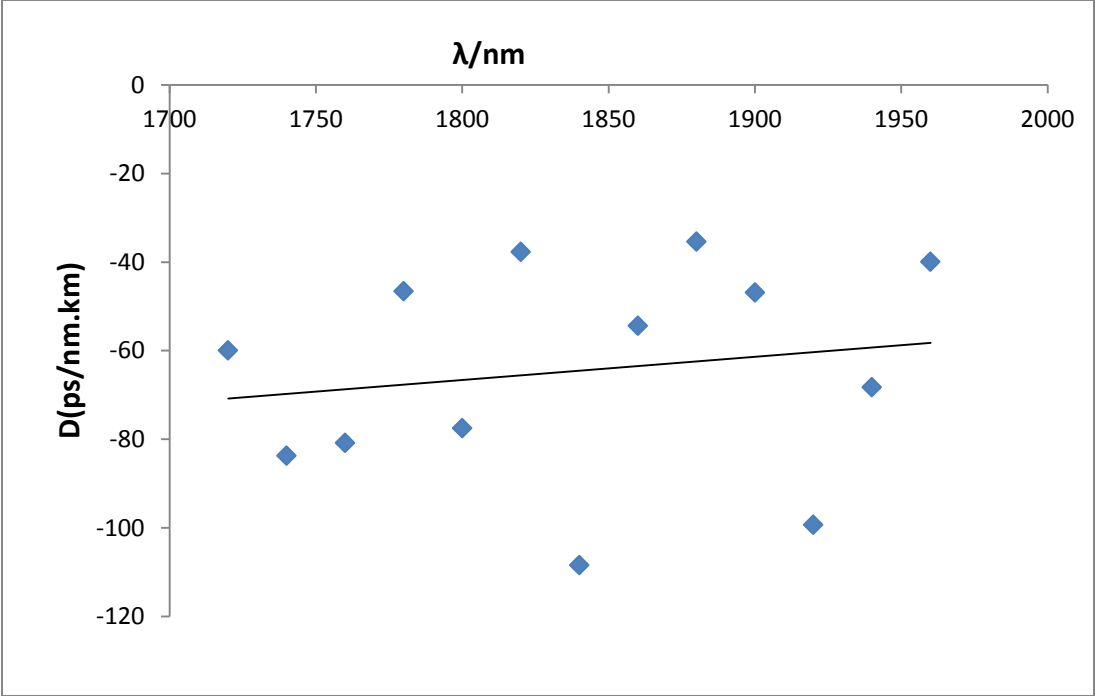
Figure 41: Dispersion distribution for the averaged core and cladding coupled modes propagating through the Ge doped fiber in the 1700nm-2000nm wavelength range.

The same averaging idea was applied in the 2150nm-2400nm to obtain the estimated average core and cladding dispersion in Ge-doped fiber. Table 9 shows the average dispersion in Ge-doped fiber in 2150nm-2400nm wavelength range due to core and cladding coupled modes.

λ ± 2.5nm	l ± 0.0001mm	dl/mm	dλ/nm	dL/dλ	D/ps/nm.km
2300	12.1004	-0.1798	10	-17980	-46
2310	12.0305	-0.1398	10	-13980	-32
2320	12.0050	-0.051	10	-5100	-24
2330	11.9805	-0.049	10	-4900	-23
2340	11.9605	-0.04	10	-4000	-19
2350	12.0105	0.1	10	10000	48
2360	12.0704	0.1198	10	11980	57
2370	12.0205	-0.0998	10	-9980	-28
2380	11.9608	-0.1194	10	-11940	-22

Table 9: Dispersion in Ge-doped fiber in the 2150nm-2400nm wavelength range

Similarly by combining the obtained dispersion results in the two wavelength ranges, the dispersion trend in 1700nm-2400nm was obtained as shown in Figure 42 below. It's observed that Ge-doped fiber exhibits negative dispersion (normal dispersion) in 1700nm-2400nm wavelength range and its dispersion increases with increasing wavelength. We can also estimate zero dispersion wavelength for this fiber. From Figure 42, zero dispersion wavelength lies between 2400nm-2500nm.
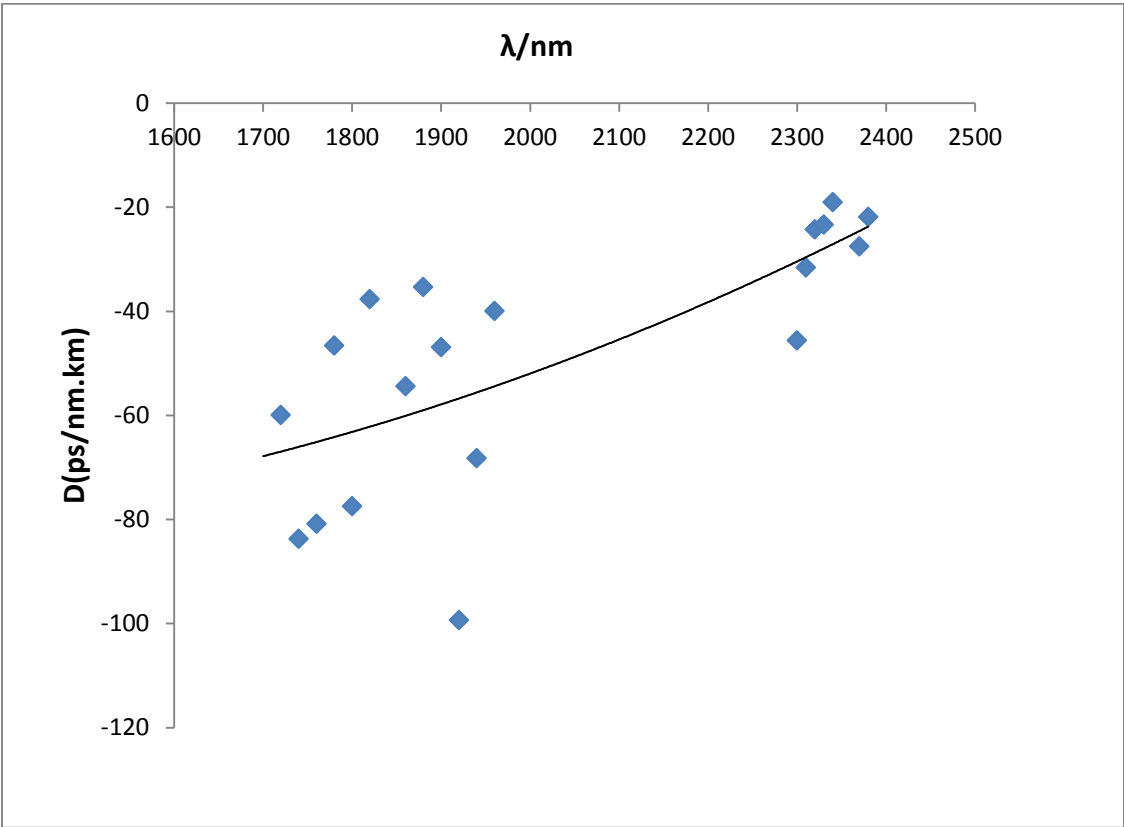
Figure 42: Dispersion distribution in Ge-doped fiber in 1700nm-2400nm wavelength range for the core and cladding coupled modes

4.1.3 Yb:Tm doped fiber

The same multi-maxima situation observed in Ge-doped doped fiber was also observed in Yb:Tm doped fiber. The length of fiber used during measurements was 75cm. In addition to core mode, several cladding modes also existed in Yb:Tm-doped fiber as a result of core-cladding coupling which led to several maximum interference points for a particular wavelength.

Table 10 shows the different maxima observed as a results of several mode propagation through the Yb:Tm doped fiber in the 1700nm-2000nm wavelength range. Approximately three maxima were observed in this wavelength range as shown below.

$\lambda \pm 2.5nm$	$l1 \pm 0.0001mm$	$l2 \pm 0.0001mm$	$l3 \pm 0.0001mm$
1700	14.3397	14.5396	
1720	14.3497	14.4396	
1740	14.4196	14.8497	14.9489
1760	14.5599	14.6299	14.7299
1780	14.6399	14.7873	14.9188
1800	14.7697	14.9596	15.1394
1820	14.7899	14.8784	14.9789
1840	14.8285	15.0584	15.1993
1860	15.0575	15.2380	
1880	15.0195	15.3277	15.4279
1900	15.1488	15.4783	15.7592
1920	15.1997	15.3296	15.6892
1940	15.3995	15.4709	15.8291
1960	15.3895	15.6575	15.9290
1980	15.6694	16.0091	

Table 10: Paths length for different modes observed in Yb:Tm-doped fiber due to core and cladding coupled mode propagation in the 1700nm-2000nm wavelength range.

Figure 43 shows that the points of maxima in table 10 correspond to different modes propagating through the fiber. They are both core modes and core-cladding coupled modes.
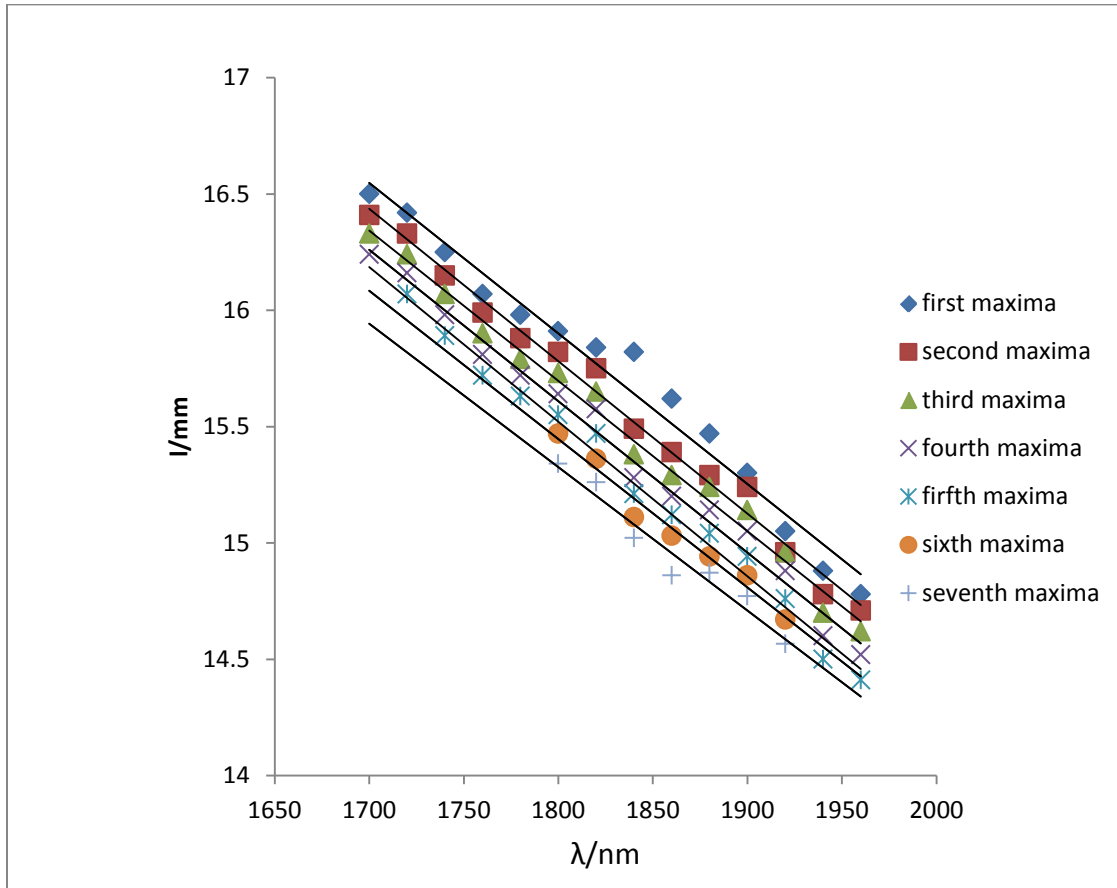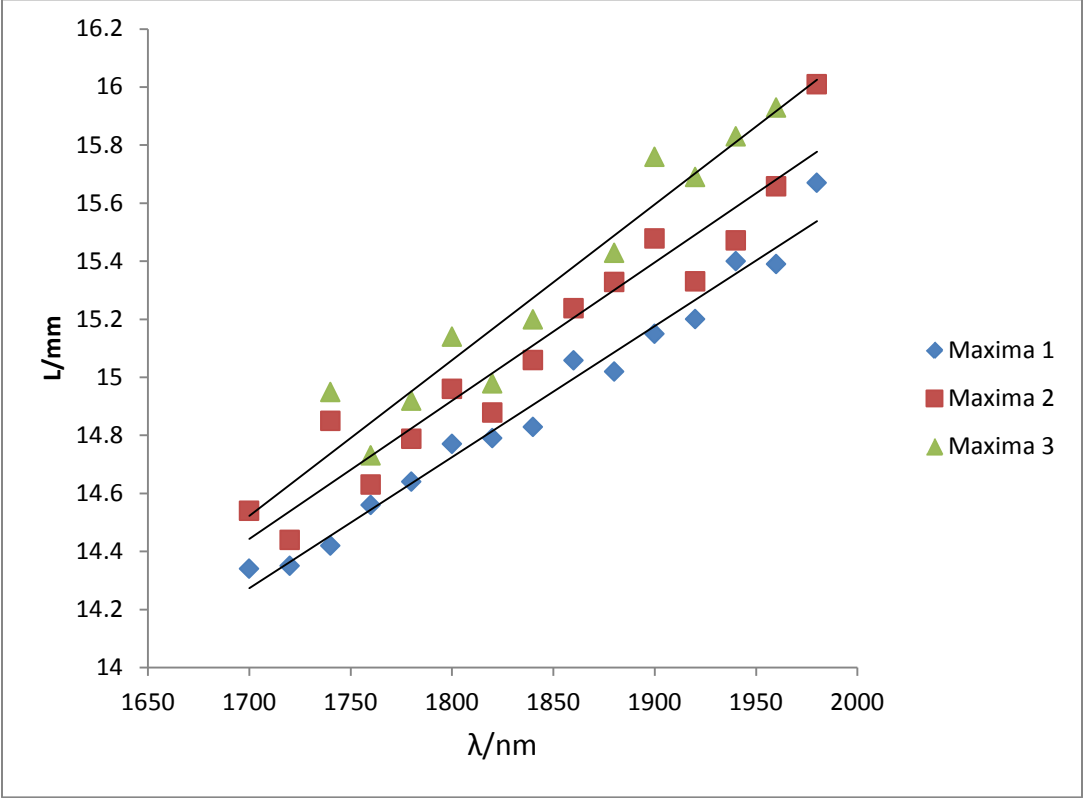

Figure 43: Path lengths for different modes propagating through the Yb: Tm-doped in the 1700nm-2000nm wavelength range

Figure 44 shows the average dispersion results for core and cladding coupled modes propagating through the Yb:Tm doped fiber in 1700nm-2000nm wavelength range. The dispersion coefficient is positive (anormalous dispersion) for this type of fiber in this wavelength range.
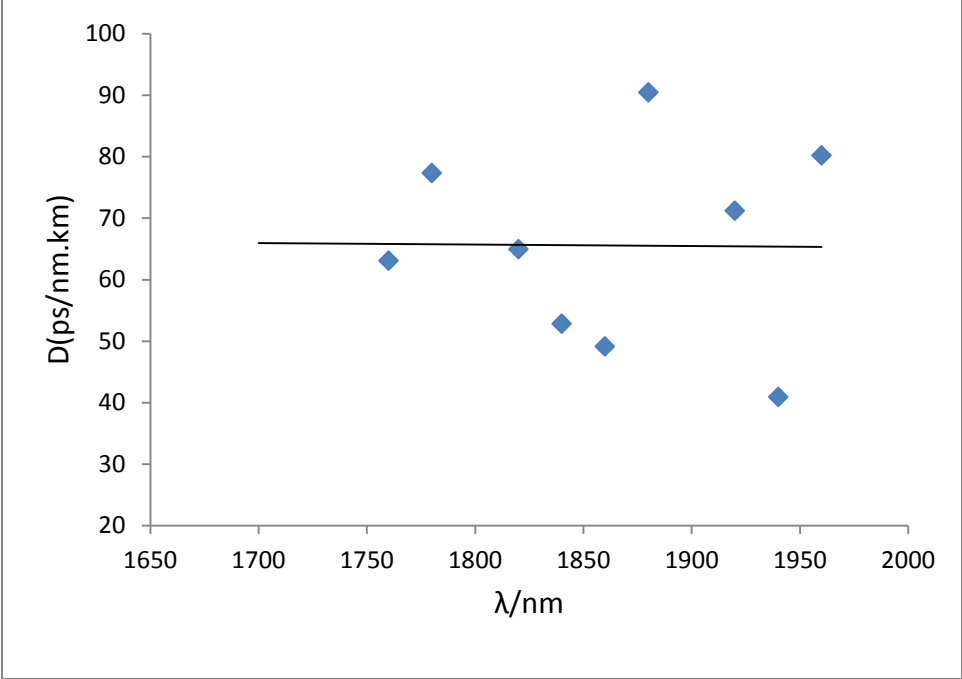
Figure 44: Dispersion distribution for the average of the modes propagating through Yb: Tm-doped fiber in the 1700nm-2000nm wavelength range.

Table 11 shows the different maxima observed as a results of several mode propagation through the Yb:Tm doped fiber in the 2150nm-2400nm wavelength range. Approximately six maxima were observed in this wavelength range. The several maxima observed were also a combination of both the core and cladding coupled modes.

λ $\pm 2.5 nm$	l1 $\pm 0.0001 mm$	l2 $\pm 0.0001 mm$	l3 $\pm 0.0001 mm$	l4 $\pm 0.0001 mm$	l5 $\pm 0.0001 mm$	l6 $\pm 0.0001 mm$
2300	10.6998	11.2193				
2310	10.7398	11.0395	11.9186	11.8687	12.2683	12.5880
2320	10.9895	11.2692	11.9286	12.2083	12.5780	
2330	11.0095	11.4690	11.6689	12.1883	12.5580	
2340	10.8397	11.0195	11.5790	11.8986	12.1983	12.5180
2350	11.0495	11.3292	11.9686	11.9586	12.5080	13.0170
2360	11.1194	11.6089	11.9286	12.4381	12.6979	13.2671
2370	11.6189	12.0185	12.1784	12.5180		

Table 11: Paths length for different modes observed in Yb:Tm-doped fiber due to several mode propagation in the fiber in the 2150nm-24000nm wavelength range

When the maximum interference points in Table 11 above were plotted against wavelength, Figure 45 was obtained. Figure 45 shows that these points of maxima in table 11correspond to different modes propagating through the fiber. This was because each mode has a different paths length at a particular wavelength as depicted by the figure.
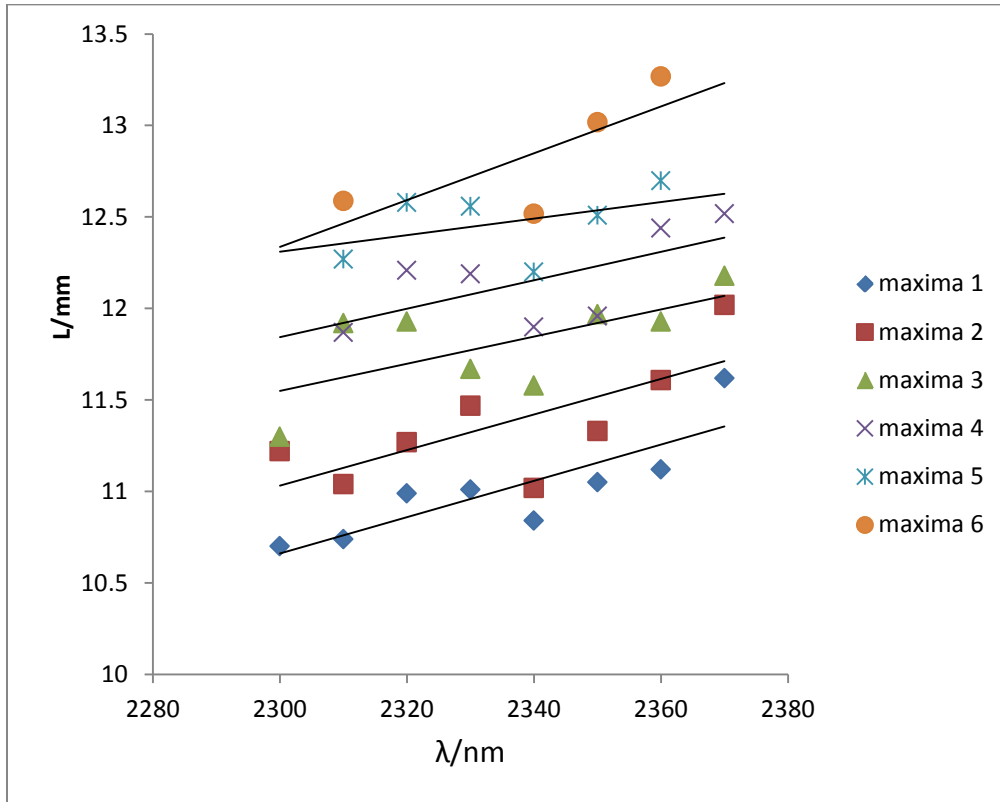
Figure 45: Path lengths for different modes propagating through the Yb: Tm-doped fiber in the 2150nm-24000nm wavelength range

Figure 46 shows the averaged dispersion due to core and cladding modes propagating through the Yb:Tm doped fiber in 2150nm-2400nm wavelength range. The fiber also exhibits anomalous dispersion which increases with increasing wavelength in this wavelength range.
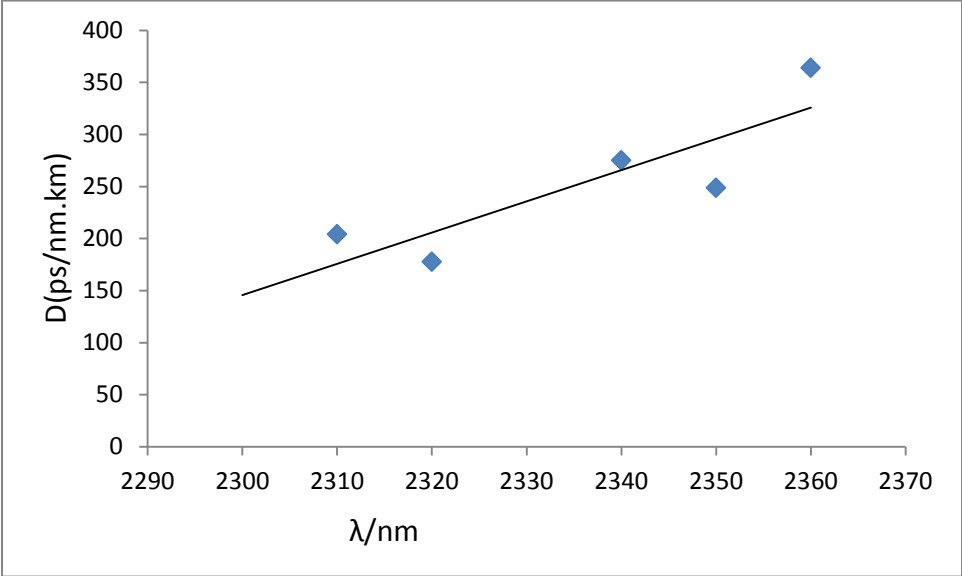
Figure 46: Dispersion for the different modes propagating through Yb: Tm-doped fiber in the 2150nm-24000nm wavelength range.

By combining the obtained dispersion results in the two wavelength ranges, the dispersion trend in 1700nm-2400nm was obtained as shown in Figure 47. The dispersion increases with increasing wavelength in this wavelength region and its positive for Yb:Tm doped fiber.
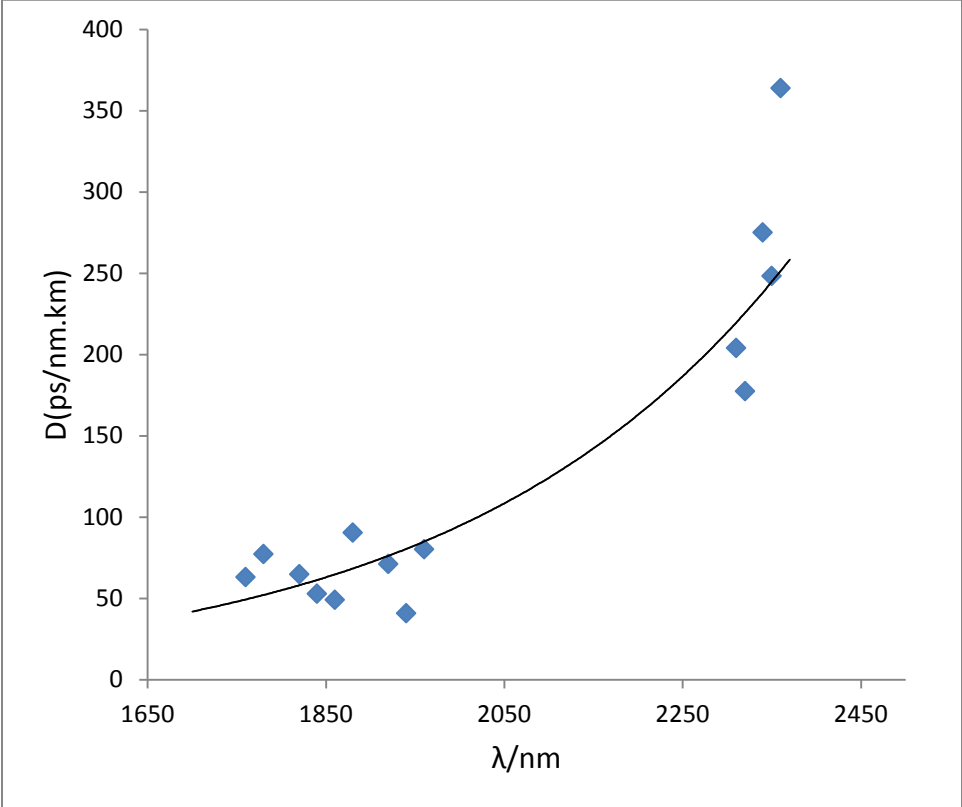
Figure 47: Dispersion in Yb:Tm-doped fiber in 1700nm-2400nm wavelength range.

Chapter Five: Discussion, Recommendations and Conclusion

5.1. Discussion

5.1.1. Standardization of the setup

In order to test how good the experimental results are, it is important to link theory and experiment. A silica fiber of SMF-28 type drawn at NTNU fiber tower with similar composition as the standard silica telecommunication fiber (SMF 28) was used to test the setup. SMF 28 has been studied thoroughly by different groups of people and therefore its properties and dispersion are clearly known. The theoretical data were obtained from the Fiber Optical Research Center (FORC), Russian academy of sciences. Dispersion was measured in the wavelength ranges 1700nm-2000nm and 2150nm-2450nm. The measured dispersion results and the theoretical calculation results are in good agreement as shown in Figure 36. This testifies the reliability of the results obtained in the setup and the similarity of the properties of NTNU-drawn silica fiber in comparison with SMF 28

Dispersion is seen to increase with increasing wavelength in 1700nm-2450nm wavelength range in the silica fiber drawn at NTNU. This fiber exhibits anomalous dispersion.

The dispersion coefficient values for silica fiber drawn at NTNU vary slightly from the theoretically obtained results for the standard telecommunication fiber, though keeping the tendency and the slope of the curve. The difference could be as a result of slight variations in the chemical composition of the fiber and the uncertainty of the wavelength selection by a monochromator. The chemical composition could not be 100% similar to that of the standard telecommunication fiber. But all in all, the silica fiber drawn at NTNU is a good comparison to the SMF 28.

The average measured dispersion in the 1700nm-2000nm wavelength range was 32 ± 4 ps/km.nm compared to the theoretical average result of 31ps/km.nm. This testified how good the setup is. In the 2150nm-2450nm wavelength range, the measured average dispersion was 65 ± 7 ps/km.nm. The precision of the measured dispersion was based on the largest estimated uncertainty in the measurements which was from the selection of wavelength by the monochromator. Considering the monochromator minimum reading of 20nm, we estimate the uncertainty in the wavelength selection as $\pm 2.5 nm$ that resulted in the dispersion coefficient uncertainty of about 4ps/nm.km. The results for 2150nm-2450nm spectral range exhibit higher

error, and this is as a result of a longer coherence length of Cr:ZnS laser source in comparison with superluminiescent Tm-doped fiber source.

5.1.2. Manual versus Auto dispersion setup

Automation of the measurements was the important task of the project, so the influence of the automation on the results of the measurements has to be defined. Results show that the manual and computer controlled setup dispersion results are in agreement with each other. The computer controlled measured results give a bit closer approximate to the theoretical than the manual results as shown in Figure 36. Considering the silica fiber length of 75cm, the measured average dispersion with auto setup was 32 ± 4ps/km.nm and 34 ± 4ps/km.nm with the manual setup in the 1700nm-2000nm, in comparison with the average theoretical value of 31ps/km.nm.

Nevertheless the precision of the measurements were just the same for both detection mechanisms giving the error of about 4ps/km.nm. At the same time, the reproducibility of the detection of the interference maximum was greatly increased due to automation, dropping from average error of 10-15µm for manual detection to not more than 0.5µm for automatized setup. It became clear that the main uncertainty in the measurements now originates from the reproducibility of the wavelength detection by the monochromators. The currently used grating monochromators has the minimal wavelength reading of 20nm and gives no possibility for automation of the wavelength selection. Substituting it with a grating monochromator with subsequent automation of the wavelength selection will result in the gradual improvement of precision of the dispersion results.

Furthermore, the realized automation results in the great increase of the speed of the measurements and reduces the probability of human errors. In the auto regime, once the run button is pressed, the spectral interference region is scanned from the beginning to the end, and then motor steps back to a position corresponding to the point of maximum for a selected wavelength from the monochromotor. These auto results are more reliable because for every wavelength selected, the whole spectral interference region is scanned thus one is assured that the selected point of maximum is the right maximum interference point. This regime of the setup saves time because one only needs to select the wavelength and wait for the result.

It is now possible to increase precision of the measurements by realizing the several measurements runs one after another keeping the same time consumption.

5.1.3 Shortest fiber length measured by the current setup

The setup is able to measure short length fibers (normally 70cm to 250cm). From Figure 38, when the length of the silica fiber was decreased to 75cm, the obtained results agreed with 207cm fiber length results. However, the decrease of the fiber length results in the higher noise. The shorter fiber we measure, the closer are the interference maxima points for the neighboring wavelength to one another, and the precision of the position detection then comes into play. This means that it's better to take longer fibers to increase the precision.

Even shorter fiber lengths (up to 40cm) could be measured by the setup. The position modulation speaker and mirror reflectors in this case have to be adjusted to decrease the length of the air arm. Up to 40cm fiber length can be measured by the setup. This shows how good this setup is compared to other measurement dispersion setups that need several kilometers of fibers for measurements. Thus for cases where cost of fiber is more important than precision, fiber length of less than 1m can be used, but for precision preferences, fiber length of 1.0-2.5m can be used in the current setup.

5.1.4 Ge- doped fiber

Fiber length of 70cm was used for measurements. Dispersion in Ge-doped doped fiber is negative in the 1700-2400nm wavelength range as shown in Figure 42. The average measured dispersion is approximately -47 ± 5ps/km.nm in the 1700-2000nm wavelength range and -28 ± 5ps/km.nm in the 2150nm-2400nm wavelength range.

The fiber is single mode but there are several maxima observed at a particular wavelength. This shows that there are several modes propagating through the fiber. The other modes propagating through the fiber are probably cladding modes coupled from the core into the cladding and coupled directly into the cladding because of the small core size of the fiber (about 3µm).

By taking into consideration of all the maxima and analyzing them as shown in figure 40, we observe clear picture of several modes (cladding modes). Typically 6-7 maxima were observed for a particular wavelength. All these modes exhibit almost a similar dispersion pattern which makes it relatively hard to identify the core mode. In our calculations, we simply averaged all the modes to obtain the rough estimation of the fiber dispersion. The precise measurements would require the elimination of all the cladding modes that is out of scope of this thesis.

Figure 41 results after averaging the core and cladding coupled modes in the 1700nm-2400nm wavelength range. The same idea was used in the 2150nm-2400nm wavelength range resulting

into Figure 42. From this figure, it's observed that dispersion increases with increasing wavelength in the 1700nm-2400nm wavelength range and the zero-dispersion wavelength can be estimated to lie between 2400nm-2500nm.

Application

Ge-doped fiber can be used as dispersion compensation element in the Ge-doped fiber laser for ultrashort pulsed operation regime.

5.1.5 Yb:Tm doped fiber

The length of fiber used for measurements was 75cm. There is multimode propagation through the fiber since also several maxima were observed at a particular wavelength as shown in Figures 44 and 45. Since the fiber is considered as single mode, we consider the extra modes to be cladding modes guided inside the cladding and coupled from the fiber core into the cladding.

The average measured dispersion in Yb:Tm-doped fiber was approximately 70 ± 5ps/km.nm in the 1700-2000nm wavelength range and 226 ± 21ps/km.nm in the 2150nm-2400nm wavelength range.

In the 1700nm-2000nm, LCT-10 (Yb:Tm doped fiber with 0.7% of Tm) yielded no results because of absorption by Tm. However when a lower concentration of Tm (LCTP1) of 0.4% was used, results were obtained, though still absorption occurred which limited the signal through the fiber arm of the interferometer. This fiber is characterized by positive dispersion according to the experimental results obtained.

Application

Yb:Tm doped fiber can be used as active medium for fiber lasers. Thus the dispersion information can be used to compensate for dispersion in the fiber laser if we are to achieve really ultra-short pulses. In addition, Yb:Tm doped fiber laser can be used in place of Tm-doped fiber lasers. This is advantageous because Yb:Tm doped laser can be pumped at 980nm laser diode. These laser diodes are much cheaper and higher power is available compared to 1550nm or 800nm laser diodes that can be used to pump Tm-doped doped fiber laser. The basic idea involves pumping Yb ions which deliver the energy to Tm ions.

Another application of Yb:Tm doped fiber laser is light emitters for visualization application. This is because Tm emits not only at 2000nm but also in the blue region.

5.1.6 Error analysis

Errors in the experiment were mainly from the measurement instruments, surrounding environment and the light beam guiding components as described below.

Uncertainty from measurement instruments

The uncertainty in the measured dispersion was estimated using Gauss error propagation. From equation (45), the Gauss error propagation formula from which the uncertainties in dispersion were estimated is:

$$\Delta D(\lambda) = [\sqrt{(\frac{\Delta L}{L})^2 + (\frac{\Delta(d\Delta l)}{d\Delta l})^2 + (\frac{\Delta d\lambda}{d\lambda})^2}] \; D(\lambda) \;) \qquad\qquad (46)$$

Where ΔL, $\Delta(d\Delta l)$, and $\Delta(d\lambda)$ are the uncertainties in the measurement of fiber length L, path length difference (accuracy of the step motor) Δl, and wavelength change $d\lambda$, respectively. $\Delta D(\lambda)$, is the second order dispersion uncertainty to be estimated. Typical uncertainty estimates used in the calculations were $\Delta L = \pm 0.0005m$, $\Delta(d\Delta l) = \pm 0.1 \mu m$, and $\Delta d\lambda = \pm 2.5 nm$. The calculated average dispersion uncertainties were: $\pm$4ps/km.nm for dispersion measurements in silica fiber in both 1700nm-2000nm and 2150nm-2400nm wavelength ranges, $\pm$5ps/km.nm for Ge-doped fiber in both 1700nm-2000nm and 2150nm-2400nm wavelength ranges and $\pm$5ps/km.nm in 1700nm-200nm and $\pm$21ps/km.nm in 2150nm-2400nm for Yb:Tm-doped fiber.

It is worth noting that the accuracy of the results was limited majorly by the minimal wavelength reading of the monochromator used for selection of wavelength which was 20nm that lead to errors in wavelength reproducibility.

Accuracy of the results was also affected by the step size of the motor used. This was evident in Figure 37. The 0.001mm step size of the motor approximates the theoretical calculation results more accurate than the 0.01mm step size. However, both results for 0.001mm and 0.01mm step size were in agreement with each other which showed repeatability of the auto setup. Also like for any other motor, backlash is an issue. It's typically $10 \mu m$ for TRA25PPD stepper motor. However, this is avoided by stepping past the required position and then stepping back.

Errors from beam guiding components and surrounding environment

There was dispersion by the objective lens used in the fiber arm and optical losses in the experiment. However, this was not taken into account because the thickness of the components was negligible compared to the arms of the interferometer thus their dispersion being negligible. There was also water absorption in the air parts of the interferometer.

Other errors were a result of coupling inefficiencies due to poor focusing and bad cleaved ends of the fiber. Cleaving of the fiber must be done with care, this is because if the ends of the fiber are not cleaved at 90^0, coupling of light through the fiber might be difficult thus affecting the signal through the fiber. Very precise focusing of the laser into the fiber is required to avoid coupling into the cladding and precise focusing into the fiber is at a point when the output signal through the fiber is very sensitive to the focusing adjustments.

Also the signal at the boundaries of the spectrum of the source was week which makes the interference signal at the boundaries almost comparable to the noise. Thus the dispersion results at the boundaries are noise interfered.

5.2. Recommendations

It is worth noting that although the precision in the position measurement was improved in the auto regime of the setup, results are still affected by the low reproducibility of the monochromator reading used for wavelength selection. The minimal reading of the monochromator was 20nm. Results could be improved if a grating monochromator with a better precision was used.

The automation phase could be extended by automatizing the wavelength selection. In this case, the measurements could be done in the fully automatic setup. Automation of the monochromator was not achieved because of lack of proper grating as it was proposed in the beginning. However this could be easily integrated into the current auto setup by controlling the grooving of the grating with the stepper motor too.

Also enclosing the setup in a closed box can help to reduce water absorption in the arms of the interferometer and make the setup more compact. In addition fiber length of approximately 40 cm can lead to compacting the setup to about 50X40cm box. Adjusting the properties of the

source, particularly the Cr:ZnS laser source can shorten the coherence length thus enabling precise location of interference maxima. This would help improve on the results obtained in the 2150nm-2400nm wavelength range.

5.3. Conclusion

A dispersion measurement setup for short length fibers based on Mach-Zehnder interferometer was modified from manual regime to computer controlled regime. Programing of the components was written based on LabView software because of easy compatibility of components with LabView. Test of the setup was performed using standard telecommunication fiber and the obtained results indicate that the auto regime gives more accurate and precise results in addition to reliability of the results as well as faster and more user friendly method. Dispersion was measured using the two available broad band sources: superlumineiscent Tm-doped fiber source and the mode locked Cr:ZnS laser covering 1700nm-2400nm wavelength range. In addition to the standard silica fiber, dispersion in new optical fibers such as Ge-doped fiber, Yb:Tm doped fiber , Tm-doped fiber was measured by the setup, although the Tm -doped fiber didn't yield results in the 1700nm-2000nm wavelength range because of Tm absorption at this wavelength.

The measured auto setup average dispersion of silica fiber was 32 ± 4ps/km.nm and 34 ± 4ps/km.nm with the manual setup in the 1700nm-2000nm which is in good agreement with the average theoretical value of 31ps/km. This shows how good and reliable the setup is. In the 2150nm-2450nm wavelength range, the measured average dispersion in silica fiber was 65 ± 7 ps/km.nm. Similarly, the average measured second order dispersion in Ge-doped fiber was approximately -47 ± 5ps/km.nm in the 1700-2000nm wavelength range and -28 ± 5ps/km.nm in the 2150nm-2400nm wavelength range. In Yb:Tm doped fiber it was approximately 70 ± 5ps/km.nm in the 1700-2000nm wavelength range and 226 ± 21ps/km.nm in the 2150nm-2400nm wavelength range. These obtained results constitute a valuable knowledge and can be useful for development of the ultra-short pulsed fiber lasers. Fiber length between 40 cm-250 cm can be measured by the setup, although precision is lost as the fiber shortens and the maximum interference points become very close to one another. Short length fiber (down to about 40 cm) makes the setup compact. Generally, the bottleneck of the setup in its current form is the monochromator, which should be substituted for the grating one with a good wavelength

selection reproducibility and ability to be automated. Ge-Tm and Yb:Tm doped fibers could be subsequently used for development of novel ultra-short pulse fiber lasers at 2µm spectral range. Yb:Tm doped fiber laser has certain advantages over Tm doped fiber laser because cheap high-performance pumping laser diodes (at 980nm) for pumping of Yb-ions are commercially available and can significantly reduce the cost of the laser.
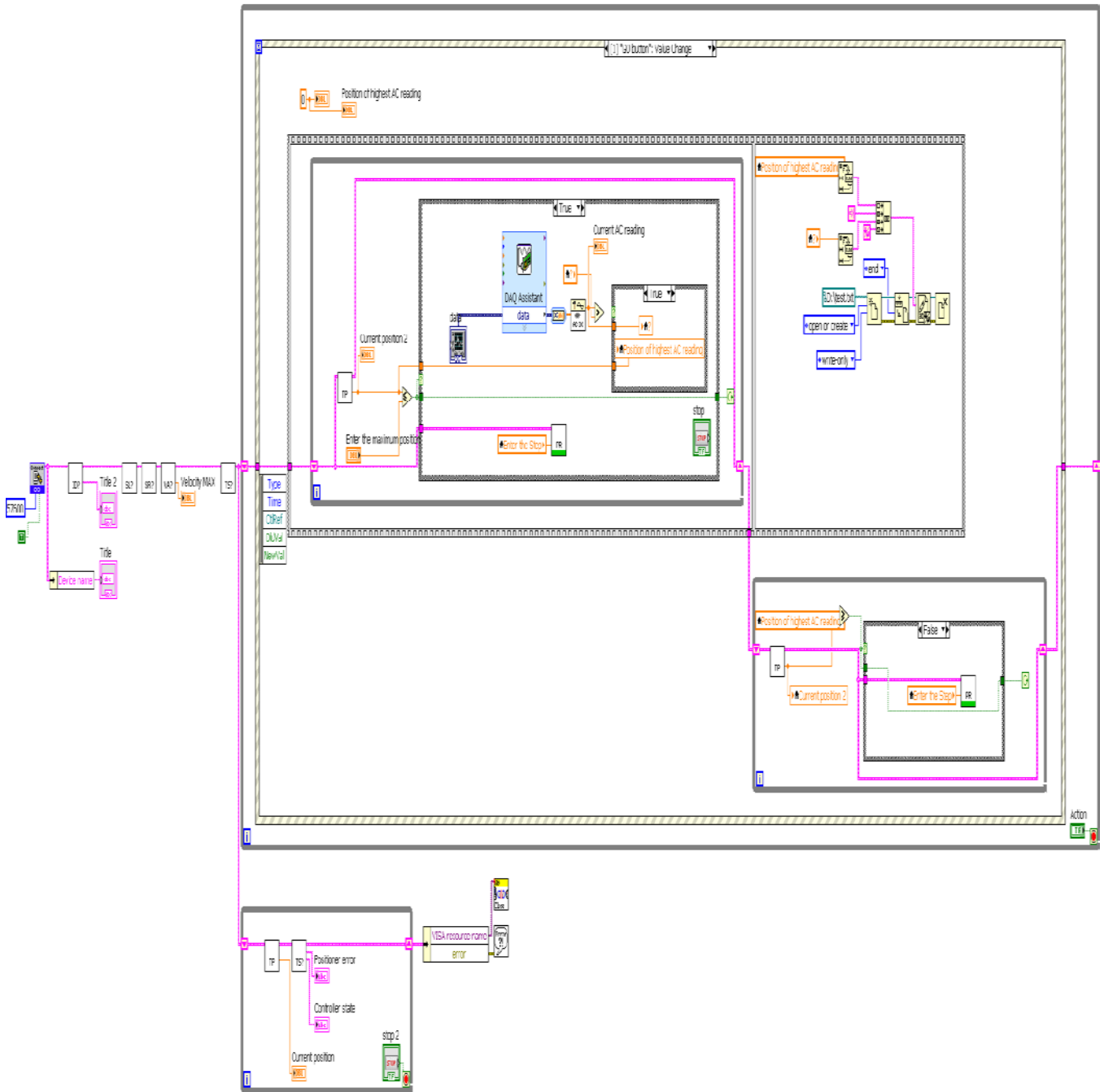
Appendix

Figure 48: Labview program that computer controls the dispersion measurement setup.

References

[1] Aegis School of Telecommunication, ''Fiber Optics Concepts'', (Accessed: 2014.04.14)

URL:http://www.aegisedu.org/mptm/s04b03t01/ofcf/ebooks/EDPFOC.htm

[2] Optical Systems Design, URL: http://osd.com.au/how-far-can-you-go/, (Accessed: 2013:01:27)

[3] M. J. Adams, "*An Introduction to Optical Waveguides*," John Wiley & Sons, Inc., New York, (1981)

[4] D. Davison, "*Single-mode wave propagation in cylindrical optical fibers in Optical Fiber Transmission''*, Edited by E. E. Basch, Indianapolis, Howard W. Sams & Co., Chapter 3, (1987)

[5] Thyagarajan, K. and A.K. Ghatak, ''The fiber optic essentials'', *IEEE Press*. xiii,242 s. : ill. (2007).

[6] B. E. A.Saleh, M. C. Teich,"*Fundamentals of photonics*", Chicester, Wiley (2007)

[7] A. Ghatak, K. Thyagarajan, ''Introduction to Fiber Optics'', Cambridge University Press, (1998)

[8] F.Träger, "*Springer Handbook of Lasers and Optics*", New York, NY, Springer Science+Business Media, pg. 419-499, (2007)

[9] Optical Communications Technolgy at Technische Universitaet Hamburg-Harburg (TUHH) (Accesed: 2013.02.18) URL: http://www.tuhh.de/okt/Forschung/Pmd/

[10] G. P. Agrawal, ''*Fiber-Optic Communication Systems''*, 3rd ed. Wiley-Interscience, (2002)

[11] P. Merrit, R. P. Tatam, and D.A. Jackson, "Interferometric chromatic dispersion measurements on short lengths of monomode optical fiber," *IEEE J. Lightwave Technol*. 7, 703-716 (1989)

URL: http://cp.literature.agilent.com/litweb/pdf/5989-2325EN.pdf

[12] P.L. Francois, M. Monerie, C. Vassallo, Y. Durteste, and F. R. Alard, " Three ways to implement interferencial techniques: Application to measurements of chromatic dispersion, birefringence, and non-linear susceptibilities'', *Journal of Lightwave Technology*, vol. 7, no. 3, pp. 500–513, (1989)

[13] G. P. Agrawal, ''Fiber-Optic Communication Systems'', 3rd Ed. New York USA: John Wiley & Sons, Inc. (2002)

[14] D. Martin ''Characterization of Optical Fibers in the Mid-Infrared'', Wien, (2005)

[15] EIA/TIA-455-169A (FOTP-169), "Chromatic dispersion measurement of single mode optical fiber by the phase shift method", (1999)

[16] EIA/TIA-455-168A (FOTP-168), ''Chromatic Dispersion Measurement of Multimode Graded-Index and Single-Mode Optical Fibers by Spectral Group Delay measurement in the time domain'', (1992)

[17] L. G. Cohen, "Comparison of single-mode fiber dispersion measurement techniques," *IEEE J. Lightwave Technol*. 3, 958-966 (1985).

[18] D.Klimentov, N. Tolstik, V.V. Dvoyrin, V.L.Kalashnikov, and I.T. Sorokina, ''Broadband dispersion measurements of ZBLAN, Germanate and Silica Fibers in MidIR '', *Journal of light*, VOL.30, NO.12, (2012)

[19] Agilent White Paper, "Agilent 86038B photonic dispersion and loss analyzer," (2007)

[20] L. Cherbi, M. Mehenni, and R. Aksas, "Experimental investigation of the modulation phase-shift method for the measure of the chromatic dispersion in a single-mode fiber coiled on a cover spool," *Microw Opt. Technol*. Lett 48, 174-178 (2006)

[21] H. Chen, ''Simultaneous measurements of non-linear coefficient, zero-dispersion wavelength and chromatic dispersion in dispersion-shifted fibers by four-wave mixing'', Optics Communications, 220, p. 331-335 (2003)

[22] T. Hasegawa, T. Nagashima, N. Sugimoto, ''Determination of nonlinear coefficient and group-velocity-dispersion of bismuth-based high nonlinear optical fiber by four-wave-mixing'' Optics Communications, 281, p. 782-787 (2008)

[23] P. Hlubina, M. Szpulak, D. Ciprian, T. Martynkien, and W. Urbanczyk, "Measurement of the group dispersion of the fundamental mode of holey fiber by white-light spectral interferometry," *Opt. Express* 15, 11073–11081 (2007)

[24] R. Cella and W. Wood, "Measurement of chromatic dispersion in erbium doped fiber using low coherence interferometry," in Proceedings of the Sixth Optical Fiber Measurement Conference (OFMC'01), 207-210 (2001).

[25] C. Palavicini, Y. Jaouën, G. Debarge, E. Kerrinckx, Y. Quiquempois, M. Douay, C. Lepers, A.-F. Obaton, G. Melin, "Phase-sensitive optical low-coherence reflectometry technique applied to the characterization of photonic crystal fiber properties," Opt. Lett. 30, 361-363 (2005).

[26] J. Gehler and W. Spahn, "Dispersion measurement of arrayed-waveguide grating by Fourier transform spectroscopy," Electron. Lett. 36, 338-340 (2000)

[27] C. Palavicini, Y. Jaouën, G. Debarge, E. Kerrinckx, Y. Quiquempois, M. Douay, C. Lepers, A.-F. Obaton, G. Melin, "Phase-sensitive optical low-coherence reflectometry technique applied

to the characterization of photonic crystal fiber properties," Opt. Lett. 30, 361-363 (2005).

[28] P. Hlubina, "White-light spectral interferometry to measure intermodal dispersion in two-mode elliptical core optical fibers," Opt. Commun. **218**, 283-289 (2003)

[29] P. Hlubina, M. Szpulak, D. Ciprian, T. Martynkien and W. Urbanczyk, "Measurement of the group dispersion of the fundamental mode of holey fiber by white-light spectral interferometry," Opt. Express**15**, 11073-11081 (2006).

[30] A. B. Vakhtin, K. A. Peterson, W. R. Wood, and D. J. Kane, "Differential spectral interferometry and imaging technique for biomedical applications," Opt. Lett. **28**, 1332-1334 (2003)

[31] J. Y. Lee and D. Y. Kim, "Versatile chromatic dispersion measurement of a single mode fiber using spectral white light interferometry," Opt. Express 14, 11608–11615 (2006).

[32] P. Merrit, R. P. Tatam, and D.A. Jackson, "Interferometric chromatic dispersion measurements on short lengths of monomode optical fiber," *IEEE J. Lightwave Technol*. **7**, 703-716 (1989).

[33] P.W. Atkins, *Physical Chemistry*, 2nd Edition, Oxford University Press, Oxford, (1983).

[34]A.J.Kenyon / Progress in Quantum Electronics 26, 225-284 (2002)

[35] B. Dussardier, W. Blanc, *Proc. Optical Fiber Conf.-NFOEC*, OMN1 (2007)

[36] G. Rines, K. Wall, E. Slobodtchikov, P. Moulton, ''Efficient, high-power, Tm-doped silica fiber laser'', *Solid State Diode Laser Technol. Rev.*, pp. 229, 2008.

[37] H. Lin, S. Tanabe, L. Lin, Y.Y. Hou, K. Liu, D.L. Yang, T.C. Ma, J.Y. Yu, E.Y.B. Pun, "Near-infrared emissions with widely different widths in two kinds of Er^{3+}-doped oxide glasses with high refractive indices and low phonon energies", *J. Lum*. (2006)

[38] D. Creeden, P. A. Budni, P. A. Ketteridge, 60 W of average output power from a pulsed thulium-doped fiber amplifier operating at 2 microns, *Solid State Diode Laser Technol. Rev.*, pp. 190, (2008)

[39] V. Fomin, A. Mashkin, M. Abramov, A. Ferin, V. Gapontsev, ''3 kW Yb fiber lasers with a single-mode output'', *Int'l Symp. High-Power Fiber Lasers Appl*., (2006)

[40] D. Y. Shen, J. K. Sahu, W. A. Clarkson, ''Highly efficient Er,Yb-doped fiber laser with 188W free-running and >100W tunable output power'', *Opt. Express* 13, pp. 4916-4921, (2005)

[41] Y. Jeong, S. Yoo, C. A. Codemard, J. Nilsson, J. K. Sahu, D. N. Payne, R. Horley, P. W. Turner, L. M. B. Hickey, A. Harker, M. Lovelady, A. Piper, ''Erbium:ytterbium co-doped large-

core fiber laser with 297W continuous-wave output power'', *IEEE J. Selected Topics Quantum Electron.* 13, pp. 573-579, (2007)

URL; doi:10.1109/JSTQE.2007.897178

[42] D. Gapontsev, N. Platonov, M. Meleshkevich, A. Drozhzhin, V. Sergeev, ''415W single-mode CW thulium fiber laser in all-fiber format'', *CLEO Europe*, Post-deadline paper CP2-3-THU (2007)

[43] E. Sorokin, N. Tolstik, I. Sorokina, '' 1 Watt femtosecond Mid-IR Cr:ZnS laser'', *Proc. Of SPIE*, vol. 8599 859916-4 (2013)

[44] T. Zhang, Z. Yang, W. Zhao, Y. Wang, P. Fang, and C. Li, "Dispersion measurement of Yb-doped fiber by a spectral interferometric technique," *Chin. Opt. Lett.*, vol. 8, pp. 262–265, (2010).

[45] P. Merritt, R. P. Tatam, and D. A. Jackson, "Interferometric chromatic dispersion measurements on short lengths of monomode optical fiber," *J.Lightw. Technol.*, vol. 7, pp. 703–716, (1989)

[46] E. Sorokin, N. Tolstik, and I. T. Sorokina, "Femtosecond operation and self-doubling of Cr:ZnS laser," presented at the Nonlinear Optics: Materials, Fundamentals and Applications Conference, Kauai, HI, Paper NThC1 (2011)

[47] E. Sorokin, N. Tolstik, and I. T. Sorokina, "Kerr-lens mode-locked Cr:ZnS laser," presented at the Advanced Solid-State Photonics Conference (ASSP), San Diego,CA, Paper AW5A.5v (2012)

[48] A. Halder, M. C. Paul, S. W. Harun, S. M. M. Ali, N. Saidin,2S. S. A. Damanhuri, H. Ahmad, S. Das,1 M. Pal, and S. K. Bhadra, '' 1880-nm Broadband ASE Generation With Bismuth–Thulium Codoped Fiber'', Vol. 4, No. 6, (2012)

[49]Genesis Laboratory Systems, Inc, ''Jarrell Ash monochromators and spectrographs'', (Accessed: 2013.07.21)

URL: http://www.genlabsystems.com/jarrell_ash/gratings.html

[50] Thorlabs.com, ''ruled and reflective diffraction gratings'', (Accessed: 2014.01.17)

URL: http://www.thorlabs.de/newgrouppage9.cfm?objectgroup_id=26

[51] Newport.com, '' TRA Series, Compact Motorized Actuators'', (Accessed: 2013.08.04)

URL:http://www.newport.com/TRA-Series-Compact-Motorized Actuators/823081/1033/info.aspx#tab_orderinfo

[52] Newport.com, '' CONEX_IOD, analog/digital I/O module'', (Accessed: 2013.01.27)

URL:http://assets.newport.com/webDocuments-EN/images/15084.PDF